



HAL
open science

Multi-stage Reactive Formation of Troctolites in Slow-spreading Oceanic Lithosphere (Erro–Tobbio, Italy): a Combined Field and Petrochemical Study

Valentin Basch, Elisabetta Rampone, Laura Crispini, Carlotta Ferrando, Benoit Ildefonse, Marguerite Godard

► To cite this version:

Valentin Basch, Elisabetta Rampone, Laura Crispini, Carlotta Ferrando, Benoit Ildefonse, et al.. Multi-stage Reactive Formation of Troctolites in Slow-spreading Oceanic Lithosphere (Erro–Tobbio, Italy): a Combined Field and Petrochemical Study. *Journal of Petrology*, 2019, 60 (5), pp.873-906. 10.1093/petrology/egz019 . hal-02349556

HAL Id: hal-02349556

<https://hal.umontpellier.fr/hal-02349556v1>

Submitted on 24 Sep 2020

HAL is a multi-disciplinary open access archive for the deposit and dissemination of scientific research documents, whether they are published or not. The documents may come from teaching and research institutions in France or abroad, or from public or private research centers.

L'archive ouverte pluridisciplinaire **HAL**, est destinée au dépôt et à la diffusion de documents scientifiques de niveau recherche, publiés ou non, émanant des établissements d'enseignement et de recherche français ou étrangers, des laboratoires publics ou privés.

Multi-stage Reactive Formation of Troctolites in Slow-spreading Oceanic Lithosphere (Erro–Tobbio, Italy): a Combined Field and Petrochemical Study

Valentin Basch¹, Elisabetta Rampone^{1*}, Laura Crispini¹, Carlotta Ferrando^{2†}, Benoit Ildefonse² and Marguerite Godard²

¹DISTAV, Università degli Studi di Genova, Corso Europa 26, Genova I-16132, Italy; ²Géosciences Montpellier, University of Montpellier, CNRS, 34095 Montpellier cedex 05, France

*Corresponding author. E-mail: betta@dipteris.unige.it

†

Present address: CRPG, University of Lorraine, 54501 Vandoeuvre-les-Nancy, France.

Received June 21, 2018; Accepted March 19, 2019

ABSTRACT

Many recent studies have investigated the replacive formation of troctolites from mantle protoliths and the compositional evolution of the percolating melt during melt–rock interaction processes. However, strong structural and geochemical constraints for a replacive origin have not yet been established. The Erro–Tobbio impregnated mantle peridotites are primarily associated with a hectometre-size troctolitic body and crosscutting gabbroic dykes, providing a good field control on melt–rock interaction processes and subsequent magmatic intrusions. The troctolitic body exhibits high inner complexity, with a host troctolite (Troctolite A) crosscut by a second generation of troctolitic metre-size pseudo-tabular bodies (Troctolite B). The host Troctolite A is characterized by two different textural types of olivine, corroded deformed millimetre- to centimetre-size olivine and fine-grained rounded undeformed olivine, both embedded in interstitial to poikilitic plagioclase and clinopyroxene. Troctolite A shows melt–rock reaction microstructures indicative of replacive formation after percolation and impregnation of mantle dunites by a reactive melt. The evolution of the texture and crystallographic preferred orientation (CPO) of olivine are correlated and depend on the melt/rock ratio involved in the impregnation process. A low melt/rock ratio allows the preservation of the protolith structure, whereas a high melt/rock ratio leads to the disaggregation of the pre-existing matrix. The mineral compositions in Troctolite A define reactive trends, indicative of the buffering of the melt composition by assimilation of olivine during impregnation. The magmatic Troctolite B bodies are intruded within the pre-existing Troctolite A and are characterized by extreme textural variations of olivine, from decimetre-size dendritic to fine-grained euhedral crystals embedded in poikilitic plagioclase. This textural variability is the result of olivine assimilation during melt–rock reaction and the correlated increase in the degree of undercooling of the percolating melt. In the late gabbroic intrusions, mineral compositions are consistent with the fractional crystallization of melts modified after the reactive crystallization of Troctolites A and B. The Erro–Tobbio troctolitic body has a multi-stage origin, marked by the transition from reactive to fractional crystallization and diffuse to focused melt percolation and intrusion, related to progressive exhumation. During the formation of the troctolitic body, the melt composition was modified and controlled by assimilation and concomitant crystallization reactions occurring at low melt supply. Similar processes have been described in ultraslow-spreading oceanic settings characterized by scarce magmatic activity.

INTRODUCTION

Recent studies have demonstrated that melt–rock interactions can lead to extensive small-scale structural and geochemical heterogeneities within percolated mantle peridotites at different depths (e.g. Quick, 1981, 1982; Dijkstra *et al.*, 2002, 2003; Lissenberg & Dick, 2008; Soustelle *et al.*, 2009, 2010, 2014; Collier & Kelemen, 2010; Higgie & Tommasi, 2012, 2014; Tursack & Liang, 2012; Saper & Liang, 2014; Dygert *et al.*, 2016; Paquet *et al.*, 2016; Renna *et al.*, 2016; Sanfilippo *et al.*, 2017), and can act as a rock-forming process for replacive lithotypes. In extensional settings worldwide, spinel harzburgites and spinel dunites showing decoupled bulk-rock and mineral chemistry have been interpreted as the replacive products of open-system reactive melt percolation at spinel-facies depths, driven by pyroxene dissolution and olivine crystallization (e.g. Takazawa *et al.*, 1992; Godard *et al.*, 1995; Kelemen *et al.*, 1995a, 1995b, 2000, 2007; Rampone *et al.*, 2004, 2008; Piccardo *et al.*, 2007; Dick *et al.*, 2008, 2010; Rampone & Borghini, 2008; Lambart *et al.*, 2009; Liang *et al.*, 2011; Pirard *et al.*, 2013; Dygert *et al.*, 2016). In contrast, plagioclase-rich peridotites have been ubiquitously found in ophiolitic and oceanic settings and interpreted as the replacive product of melt impregnation that occurred at shallower plagioclase-facies conditions, leading to olivine dissolution and interstitial plagioclase and pyroxene crystallization (e.g. Van der Wal & Bodinier, 1996; Garrido & Bodinier, 1999; Dijkstra *et al.*, 2002, 2003; Borghini *et al.*, 2007; Rampone & Borghini, 2008; Tursack & Liang, 2012; Saper & Liang, 2014; Basch *et al.*, 2018).

Melt–rock interaction has also been increasingly invoked in the formation of the oceanic crust and described as a key geochemical process in the compositional evolution of percolating mid-ocean ridge basalt (MORB) melts, based on several lines of evidence: (1) dissolution–precipitation microstructures and geochemical zoning in lower crustal gabbros (Lissenberg & Dick, 2008; Lissenberg *et al.*, 2013; Lissenberg & MacLeod, 2016); (2) the composition of melt inclusions in lava phenocrysts (Laubier *et al.*, 2014; Coumans *et al.*, 2016); (3) peculiarities in the compositional variations of MORB, not consistent with a process of fractional crystallization alone (Collier & Kelemen, 2010; Van den Bleeken *et al.*, 2011; Paquet *et al.*, 2016; Sanfilippo *et al.*, 2016a); (4) the structural and geochemical mantle inheritance inferred in olivine-rich troctolites enclosed in the lowermost oceanic crust. These olivine-rich gabbroic rocks are thought to represent the replacive product of the interaction between a dunitic matrix and a percolating tholeiitic melt in disequilibrium with its host-rock (Lissenberg & Dick, 2008; Suhr *et al.*, 2008; Drouin *et al.*, 2009, 2010; Renna & Tribuzio, 2011; Higgie

& Tommasi, 2012; Sanfilippo & Tribuzio, 2013; Sanfilippo *et al.*, 2013, 2014, 2015a, 2016b; Rampone *et al.*, 2016; Basch, 2018; Basch *et al.*, 2018; Ferrando *et al.*, 2018). However, during the dissolution–precipitation reaction, the texture of the olivine matrix progressively evolves towards the cumulate-like poikilitic texture of an olivine-rich gabbroic rock (Suhr *et al.*, 2008; Drouin *et al.*, 2010; Basch *et al.*, 2018), thus calling for strong structural and geochemical constraints to discriminate between a magmatic and a replacive origin of the lithotype.

Previous studies have documented that the Alpine–Apennine ophiolitic peridotites record various stages of melt–rock interaction occurring at different mantle depths (e.g. Rampone & Borghini, 2008; Piccardo & Guarnieri, 2010; Rampone *et al.*, 2018). In the Erro–Tobbio ultramafic unit (Voltri Massif, Ligurian Alps), peridotites preserve microstructures and geochemical compositions indicative of a multi-stage melt–rock interaction history, related to progressive exhumation of this mantle sector from spinel-facies depths to shallow oceanic environments (Rampone *et al.*, 2004, 2005, 2016; Borghini & Rampone, 2007; Borghini *et al.*, 2007; Piccardo & Vissers, 2007; Rampone & Borghini, 2008). In places, impregnated plagioclase peridotites are found in irregular contact with a hectometre-size troctolitic body, later crosscut by troctolitic and gabbroic dykes. Previous studies have inferred a prevalent magmatic origin for these gabbroic rocks (Borghini & Rampone, 2007; Borghini *et al.*, 2007; Rampone & Borghini, 2008). In a recent study on the geochemistry of olivine, Rampone *et al.* (2016) highlighted the important role of melt–rock interaction in the origin of olivine-rich troctolites. The Erro–Tobbio peridotite–gabbro association thus appears an ideal case study to track the structural and geochemical changes in mantle peridotites progressively transforming to replacive troctolites during reactive dissolution (i.e. a dissolution–precipitation process; Liang, 2003), and to identify the role of reactive versus fractional crystallization in the origin of olivine-bearing gabbroic rocks. In this study, we present detailed field mapping of the internal structural complexity of the troctolitic body, coupled with electron backscatter diffraction (EBSD) measurements, and mineral major element analyses [by electron probe microanalyser (EPMA)] of the host spinel and plagioclase peridotite, the troctolitic body, and the gabbroic intrusions.

Major outcomes of this work are (1) a documented correlation between the textural evolution of the olivine matrix and the modification of the olivine crystallographic preferred orientation (CPO) during replacive formation of the olivine-rich troctolite and (2) the demonstrated modification of the melt composition during

the melt–rock interaction history, leading to peculiar mineral compositional trends in the gabbroic intrusions, shifted towards Mg-rich olivines and clinopyroxenes.

STRUCTURAL AND PETROLOGICAL BACKGROUND

The Alpine–Apennine ophiolites are predominantly constituted by mantle peridotites and represent lithospheric analogues of ocean–continent transition zones and slow- to ultraslow-spreading environments (Rampone *et al.*, 1997, 2004, 2008; Rampone & Piccardo, 2000; Müntener & Piccardo, 2003; Müntener *et al.*, 2004; Piccardo *et al.*, 2004; Borghini *et al.*, 2007; Manatschal & Müntener, 2009). They are thought to represent the lithospheric remnants of the narrow Jurassic Ligurian Tethys oceanic basin, opened by passive lithosphere extension and breakup of the continental lithosphere, leading to slow-spreading oceanization (Rampone & Piccardo, 2000; Manatschal & Müntener, 2009).

The Erro–Tobbio ultramafic body (Voltri Massif, Ligurian Alps, Fig. 1) exposes kilometre-scale unaltered peridotites, mostly devoid of any Alpine overprint (Bezzi & Piccardo, 1971; Chiesa *et al.*, 1975; Ernst & Piccardo, 1979; Ottonello *et al.*, 1979; Hoogerduijn-Strating *et al.*, 1990, 1993; Piccardo *et al.*, 1990, 1992, 2004; Scambelluri *et al.*, 1991; Vissers *et al.*, 1991; Borsi *et al.*, 1996; Capponi *et al.*, 1999; Rampone *et al.*, 2004, 2005), allowing the study of the pre-Alpine structural and chemical mantle evolution. The Erro–Tobbio unit is mostly made of variably serpentized spinel-bearing lherzolites and harzburgites. Previous petrological and structural studies documented a tectono-metamorphic decompressional evolution of these mantle rocks, from deep lithospheric settings ($P > 15\text{--}20$ kbar) to shallow depths ($P < 5$ kbar), with a progressive re-equilibration from spinel- to plagioclase- to amphibolite-facies conditions (Hoogerduijn-Strating *et al.*, 1990, 1993; Vissers *et al.*, 1991; Rampone *et al.*, 2005), and the development of extensional shear zones forming spinel tectonites, plagioclase-, hornblende- and chlorite-bearing mylonites, and serpentinite mylonites (Hoogerduijn-Strating *et al.*, 1993). This extension-related exhumation was accompanied by multiple episodes of melt percolation and intrusion, specifically: (1) a first open-system olivine-saturated reactive porous flow at spinel-facies conditions, leading to the dissolution of mantle clinopyroxene and orthopyroxene, and crystallization of olivine; (2) a melt–rock reaction at plagioclase-facies conditions ($< 8\text{--}10$ kbar) leading to the formation of plagioclase-bearing impregnated peridotites, by dissolution of olivine and crystallization of plagioclase \pm opx \pm cpx; (3) multiple episodes of gabbroic intrusions at shallow depths ($P < 5$ kbar) (Piccardo *et al.*, 2004; Rampone *et al.*, 2004, 2005, 2014, 2016, 2018; Borghini & Rampone, 2007; Borghini *et al.*, 2007; Piccardo & Vissers, 2007; Rampone & Borghini, 2008). Geochronological studies on gabbroic rocks from the

Alpine–Apennine ophiolites indicate a large time span of gabbroic intrusion (~ 20 Myr) in the Alpine Tethys (Rampone *et al.*, 2014, and references therein). The Erro–Tobbio gabbroic intrusions yield the oldest Sm–Nd age of the crustal gabbroic sequences within the Alpine–Apennine ophiolites with an age of 178 ± 5 Ma (Rampone *et al.*, 2014), therefore representing early melt intrusions in thinned lithospheric mantle exhumed at ocean–continent transition domains (Rampone & Piccardo, 2000; Manatschal & Müntener, 2009).

In the southeastern part of the Erro–Tobbio peridotite, the impregnated mantle peridotites are in irregular contact with a hectometre-size troctolitic body, previously described as a primitive cumulate body (Fig. 1; Borghini *et al.*, 2007; Borghini & Rampone, 2007; Rampone & Borghini, 2008; Rampone *et al.*, 2016). Gabbroic dykes crosscut all mantle structures, as well as the troctolitic body-impregnated peridotite contact (Borghini *et al.*, 2007). Rampone *et al.* (2016) recently demonstrated the important effect of olivine-dissolving, plagioclase-crystallizing melt–rock interaction on the Erro–Tobbio troctolitic body mineral compositions. This leads to significant enrichments in specific trace elements [Zr, Hf, Ti, heavy rare earth elements (HREE)], coupled with strong high field strength element (HFSE)–REE fractionation in olivine.

Previous geochemical studies documented a significant change in the melt composition between the impregnation event observed in the plagioclase peridotites (Rampone *et al.*, 2005) and the late troctolite–gabbro intrusions. Impregnating melts had an orthopyroxene-saturated light REE (LREE)-depleted signature, consistent with single depleted melt increments produced by near-fractional melting of a MORB-type asthenospheric mantle source (Piccardo *et al.*, 2004; Borghini *et al.*, 2007; Rampone & Borghini, 2008). A similar origin has been inferred for other Alpine–Apennine impregnated peridotites (e.g. Rampone *et al.*, 1997, 2008, 2018; Piccardo *et al.*, 2007). On the other hand, parental melts to the troctolitic body and late gabbroic discrete intrusions resemble normal (N)-MORB-type aggregated melts (Rampone *et al.*, 1998, 2014, 2016; Borghini & Rampone, 2007; Borghini *et al.*, 2007; Rampone & Borghini, 2008). Based on available time constraints on the extensional evolution of the Erro–Tobbio mantle (i.e. the Permian age of plagioclase-facies recrystallization documented in impregnated peridotite mylonites; Rampone *et al.*, 2005), and the Jurassic age of the gabbroic intrusions (Rampone *et al.*, 2014), melt impregnation in the plagioclase peridotites and subsequent troctolite–gabbro intrusion events were probably uncorrelated.

FIELD RELATIONSHIPS

The investigated area exposes a 500 m wide ultramafic body surrounded by serpentized high-pressure, low-temperature Alpine shear zones. The ultramafic body preserves a pre-Alpine mantle history, displaying an

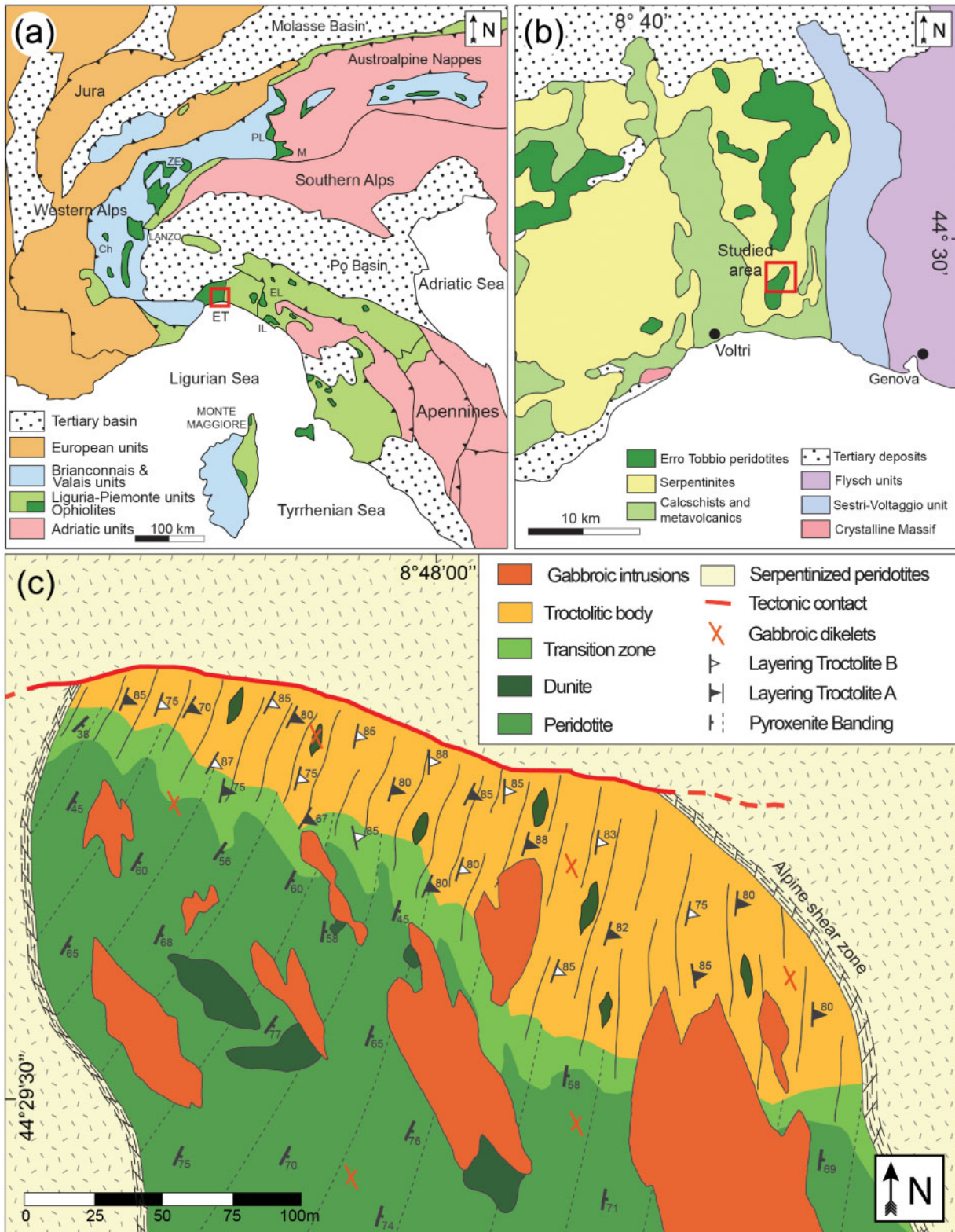


Fig. 1. (a) Sketch map of the Northern Apennines and Western Alps (redrawn after [Piccardo & Vissers, 2007](#)). The red square indicates the location of the Voltri Massif, in the Ligurian Alps. PL, Platta; M, Malenco; ZE, Zermatt; Ch, Chenaillet; ET, Ero-Tobbio; EL, External Ligurides; IL, Internal Ligurides. (b) Map of the Voltri Massif and location of the studied area within the Ero-Tobbio peridotites (redrawn after [Piccardo & Vissers, 2007](#)). (c) Geological map of the Mt. Foscallo area, in the Ero-Tobbio peridotites. This structural map merges new data measured in the field with previously published data from [Borghini *et al.* \(2007\)](#) and [Borghini & Rampone \(2007\)](#).

association between mantle peridotites and ultramafic bodies and intrusions (from plagioclase wehrlites to troctolites to olivine gabbros) (Fig. 1; Borghini & Rampone, 2007; Borghini *et al.*, 2007; Rampone & Borghini, 2008; Rampone *et al.*, 2016).

Mantle peridotites are plagioclase-bearing lherzolites showing in places a weak tectonic foliation defined by ortho- and clinopyroxene shape-preferred orientations. They are primarily associated with metre-size dunitic pods and centimetre-size pyroxenite layers showing a constant NNE–SSW orientation and strongly dipping to the east (Fig. 1). In the northernmost part of the ultramafic body, the plagioclase lherzolites are in irregular contact with a hectometre-size troctolitic body. The contact is marked by the occurrence of troctolitic and plagioclase-bearing wehrlite apophyses into the mantle peridotites, crosscutting the pyroxenite banding (Borghini & Rampone, 2007; Borghini *et al.*, 2007; Rampone & Borghini, 2008; Rampone *et al.*, 2016). Detailed mapping and sampling in selected outcrops has revealed that the inner troctolitic body is characterized by a high modal compositional variability, from plagioclase wehrlite to troctolite to dunite, and a structural complexity characterized by different generations of troctolite showing crosscutting relationships and highly variable olivine textures. In the following, based on these structural criteria, we distinguish different types of troctolites within the mafic body.

Troctolite A is in irregular contact with the mantle peridotites through a transition zone (Fig. 1) characterized by plagioclase lherzolites with decimetre-thick crosscutting troctolite and plagioclase-bearing wehrlite apophyses (Fig. 2a) in which it is difficult to easily distinguish the different lithologies (Fig. 1). Troctolite A shows variable olivine modal contents (from 55 to 74 vol. %; Table 1, Fig. 2b and c) and interstitial plagioclase \pm clinopyroxene, and it includes decimetre-size dunitic pods (Fig. 2d). The modal composition variability between olivine-rich and plagioclase-rich troctolite forms a local subvertical decimetre-size layering, showing a NNW–SSW orientation, dipping to the east (Figs 1 and 2b).

Troctolite B occurs as decimetre- to metre-size pseudo-tabular elongated bodies crosscutting the layering of plagioclase enrichment in Troctolite A (Figs 2c and 3a), and showing irregular to sharp contacts with the host troctolite (Figs 2c and 3a, b). Troctolite B bodies display extreme olivine textural variations at the scale of a few centimetres, from millimetre-size euhedral olivine crystals to centimetre- and decimetre-size hopper and dendritic olivine crystals (Fig. 3c–e). The olivine textural layering observed in Troctolite B, between granular and dendritic portions of the pseudo-tabular bodies (Fig. 3e), has a NNE–SSW strike and dips steeply to the east, similar to the plagioclase enrichment layering in Troctolite A (Fig. 1).

The peridotites and troctolitic bodies are both intruded by decametre-size gabbroic intrusions,

centimetre- to metre-thick troctolitic to olivine gabbro dykes and centimetre-thick dykelets, all striking NNW–SSE, and dipping to the east (40–50°; Figs 1 and 2a; Borghini & Rampone, 2007; Borghini *et al.*, 2007), although in places dykelets occur as conjugate pairs. Dykes and dykelets are in straight and sharp contact with the host-rock and show no chilled margins. They display a grain-size variability, from fine grained towards the margin of the intrusion (millimetre-size crystals), to coarse grained (centimetre-size crystals) in the core of the dyke. Figure 4 summarizes the field relationships mapped in the studied Erro–Tobbio ultramafic body, between plagioclase lherzolites, Troctolite A, Troctolite B, and gabbroic intrusions.

SAMPLING AND ANALYTICAL METHODS

We used samples of spinel lherzolites, plagioclase lherzolites, troctolites and gabbroic intrusions collected during previous petrological investigations of the studied area (Fig. 1; Rampone *et al.*, 2004, 2005, 2014, 2016; Borghini & Rampone, 2007; Borghini *et al.*, 2007), as well as newly collected samples of troctolite and gabbroic intrusions. The spinel and plagioclase lherzolites were sampled from a location near the troctolitic body, where the alteration is much less developed than elsewhere within the Erro–Tobbio peridotites. These samples were used as a structural and chemical reference for the mantle protolith prior to the formation of the troctolitic body and gabbroic dykes. Table 1 reports the modal composition of the 40 studied samples, namely three spinel lherzolites, four plagioclase lherzolites, 11 Troctolites A, one dunite pod, five wehrlite and troctolite apophyses, 10 Troctolites B, and six troctolitic to olivine gabbro intrusions. We performed structural EBSD mapping of all samples, and mineral major (EPMA) element chemical analyses of 24 samples, including two spinel lherzolites, two plagioclase lherzolites, seven Troctolites A, one dunite pod, two wehrlite and troctolite apophyses, five Troctolites B, and five troctolitic to olivine gabbro intrusions. Detailed methods for EBSD and mineral major element analyses can be found in the Supplementary Data; supplementary data are available for downloading at <http://www.petrology.oxfordjournals.org>.

PETROGRAPHY

Spinel lherzolites

These show protogranular to porphyroclastic assemblages of olivine, orthopyroxene, clinopyroxene and spinel. Olivine and pyroxenes (orthopyroxene + clinopyroxene) are deformed, and display kink bands and undulatory extinction, respectively. Clinopyroxenes and orthopyroxenes both show thin exsolution lamellae of the complementary pyroxene. Spinels are found as granular grains in the lherzolitic matrix and in orthopyroxene + spinel symplectites at the rim of orthopyroxene porphyroclasts, previously described as an effect of

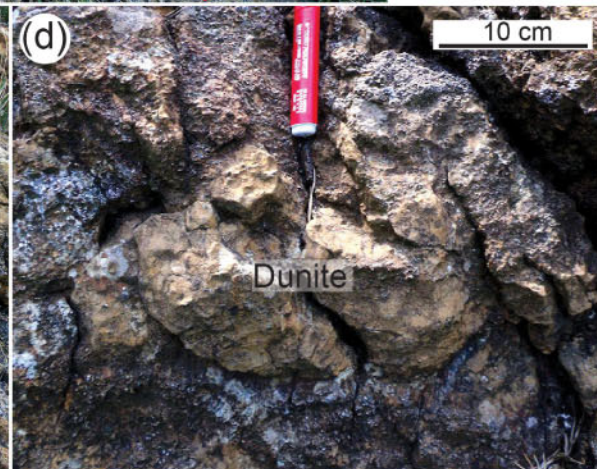
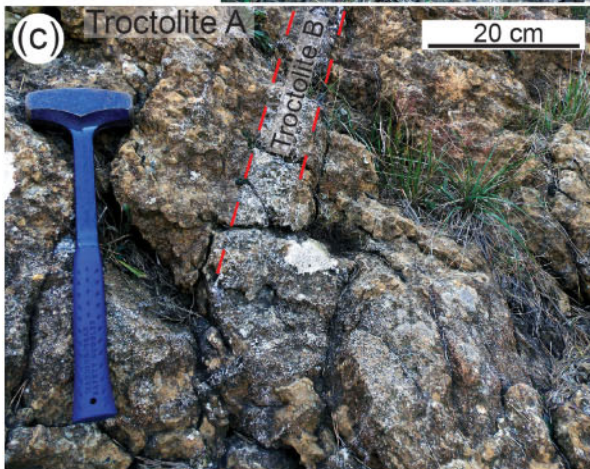
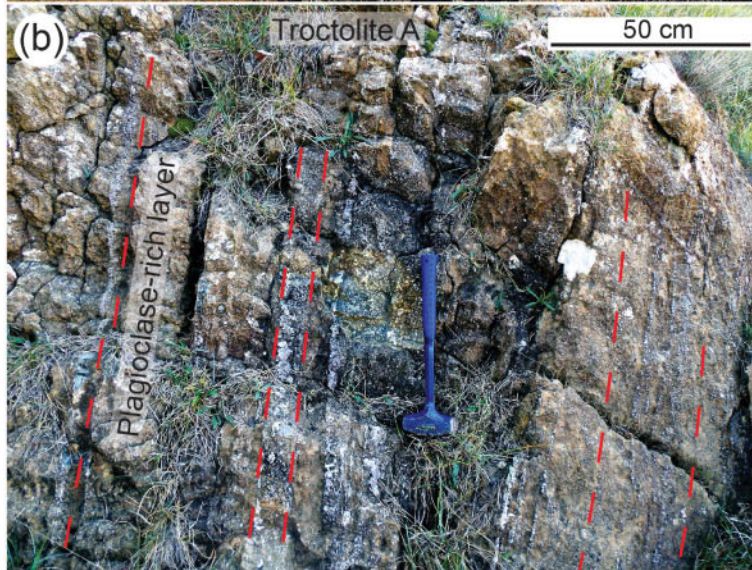


Fig. 2. Troctolite A field structures. (a) Troctolite apophysis within the mantle peridotites at the contact between the troctolitic body and the peridotites ('transition zone'), and gabbroic dyke crosscutting the association between peridotites and troctolites. (b) Plagioclase-rich layering within the host Troctolite A. (c) Crosscutting relationship between Troctolite A and Troctolite B. (d) Dunitic pod included within Troctolite A.

Table 1: Studied samples, lithotype, modal composition, and PfJ olivine

| Sample | Lithotype | Modal compositions | | | | PfJ olivine | | |
|---------|----------------------|--------------------|--------|-----|-----|-------------|-------|-------|
| | | Olivine | Plagio | Cpx | Opx | [100] | [010] | [001] |
| ETR2* | Spinel lherzolite | 78 | 0 | 7 | 15 | 2.33 | 2.84 | 2.02 |
| ETR4B* | Spinel lherzolite | 75 | 0 | 5 | 20 | 2.24 | 1.64 | 1.56 |
| ETR4A* | Spinel lherzolite | 71 | 0 | 14 | 15 | 2.08 | 1.65 | 1.32 |
| P1B* | Plagio. lherzolite | 57 | 10 | 11 | 22 | 2.12 | 3.61 | 1.50 |
| P1A* | Plagio. lherzolite | 56 | 10 | 4 | 30 | 1.90 | 2.67 | 1.40 |
| P1* | Plagio. lherzolite | 55 | 12 | 11 | 22 | 2.53 | 4.17 | 2.23 |
| MF40* | Plagio. lherzolite | 53 | 5 | 12 | 30 | 2.07 | 3.13 | 1.63 |
| MF104A | Dunite | 97 | 0 | 3 | 0 | 1.61 | 1.66 | 1.44 |
| MF21* | Troctolite A | 74 | 15 | 11 | 0 | 1.08 | 1.12 | 1.19 |
| MF15* | Troctolite A | 68 | 31 | 1 | 0 | 1.22 | 1.50 | 1.54 |
| MF97 | Troctolite A | 68 | 30 | 2 | 0 | 1.19 | 1.33 | 1.4 |
| MF51* | Troctolite apophysis | 67 | 32 | 1 | 0 | 1.77 | 1.68 | 1.88 |
| MF7A1* | Troctolite A | 66 | 23 | 11 | 0 | 1.52 | 1.58 | 1.23 |
| MF7A2* | Troctolite A | 65 | 26 | 9 | 0 | 1.39 | 1.77 | 1.21 |
| MF7C1* | Troctolite A | 65 | 27 | 8 | 0 | 1.24 | 1.40 | 1.12 |
| MF51A1* | Troctolite apophysis | 65 | 32 | 3 | 0 | 1.37 | 1.24 | 1.39 |
| MF51A2* | Troctolite apophysis | 64 | 35 | 1 | 0 | 1.25 | 1.48 | 1.41 |
| MF96A | Troctolite A | 60 | 39 | 1 | 0 | 1.14 | 1.28 | 1.17 |
| MF96B | Troctolite A | 61 | 37 | 2 | 0 | 1.25 | 1.18 | 1.13 |
| MF102A1 | Troctolite A | 60 | 36 | 4 | 0 | 1.52 | 1.42 | 1.65 |
| MF102B1 | Troctolite A | 60 | 36 | 4 | 0 | 1.19 | 1.34 | 1.42 |
| MF47A* | Wehrlite apophysis | 60 | 19 | 21 | 0 | 1.16 | 1.44 | 1.17 |
| MF47B* | Wehrlite apophysis | 59 | 13 | 28 | 0 | 1.22 | 1.47 | 1.14 |
| MF102A2 | Troctolite A | 55 | 40 | 5 | 0 | 2.58 | 1.90 | 2.06 |
| MF94B | Troctolite B | 60 | 38 | 2 | 0 | 1.11 | 1.09 | 1.07 |
| MF95A | Troctolite B | 60 | 34 | 6 | 0 | 1.21 | 1.19 | 1.23 |
| MF72Ga* | Troctolite B | 59 | 31 | 10 | 0 | 1.41 | 1.31 | 1.37 |
| MF95B | Troctolite B | 59 | 36 | 5 | 0 | 1.37 | 1.28 | 1.36 |
| MF72I* | Troctolite B | 57 | 41 | 2 | 0 | 1.15 | 1.12 | 1.21 |
| MF46A* | Troctolite B | 55 | 44 | 1 | 0 | 1.04 | 1.23 | 1.3 |
| MF73V2 | Troctolite B | 55 | 39 | 6 | 0 | | | |
| MF94A | Troctolite B | 55 | 42 | 3 | 0 | 2.50 | 1.85 | 1.85 |
| MF73V1 | Troctolite B | 50 | 48 | 2 | 0 | 1.43 | 1.40 | 1.44 |
| MF100 | Troctolite B | 45 | 51 | 4 | 0 | 1.64 | 1.88 | 1.71 |
| MF11A1* | Troctolitic gabbro | 30 | 69 | 1 | 0 | 1.08 | 1.10 | 1.3 |
| MF99 | Troctolitic gabbro | 30 | 66 | 4 | 0 | 1.06 | 1.18 | 1.17 |
| MF24* | Olivine gabbro | 27 | 59 | 13 | 1 | 1.02 | 1.13 | 1.07 |
| MF20* | Olivine gabbro | 21 | 60 | 18 | 1 | 1.02 | 1.04 | 1.05 |
| MF2B* | Olivine gabbro | 16 | 63 | 19 | 2 | | | |
| MF2A* | Olivine gabbro | 15 | 68 | 16 | 1 | | | |

Plagio, plagioclase; Cpx, clinopyroxene; Opx, orthopyroxene; PfJ, Fabric strength of single crystallographic pole.

*Samples investigated in previous studies (Rampone *et al.*, 2004, 2014, 2016; Borghini & Rampone, 2007; Borghini *et al.*, 2007; Rampone & Borghini, 2008). (See text for further details.)

cooling of the peridotites and equilibration at lithospheric temperatures (970–1100°C; Rampone *et al.*, 2005; Rampone & Borghini, 2008). The spinel lherzolites display melt–rock interaction microstructures with the development of olivine embayments replacing mantle pyroxenes (i.e. pyroxene dissolution and olivine crystallization). These microstructures, associated with an increase in olivine modal compositions, have been extensively described in the Alpine–Apennine ophiolites (Piccardo *et al.*, 2004; Rampone *et al.*, 2005, 2008; Piccardo & Vissers, 2007; Rampone & Borghini, 2008; Basch *et al.*, 2018) and in the Othris Massif (Dijkstra *et al.*, 2003), and have been interpreted as the result of a pyroxene-dissolving, olivine-crystallizing reactive melt percolation at spinel facies.

Plagioclase lherzolites

These have been previously described as the replacive product of melt impregnation of the spinel lherzolites (Borghini *et al.*, 2007). They show similar textures and microstructures to the spinel-facies protolith, but are characterized by an enrichment in undeformed interstitial plagioclase and orthopyroxene (Table 1), developing embayments on kinked olivine and exsolved clinopyroxene. These melt–rock reaction microstructures are indicative of an orthopyroxene-saturated composition of the impregnated melt, as previously described for the Alpine–Apennine ophiolitic peridotites (Rampone *et al.*, 1997, 2005, 2008, 2016, 2018; Müntener & Piccardo, 2003; Piccardo *et al.*, 2004; Borghini & Rampone, 2007; Borghini *et al.*, 2007;

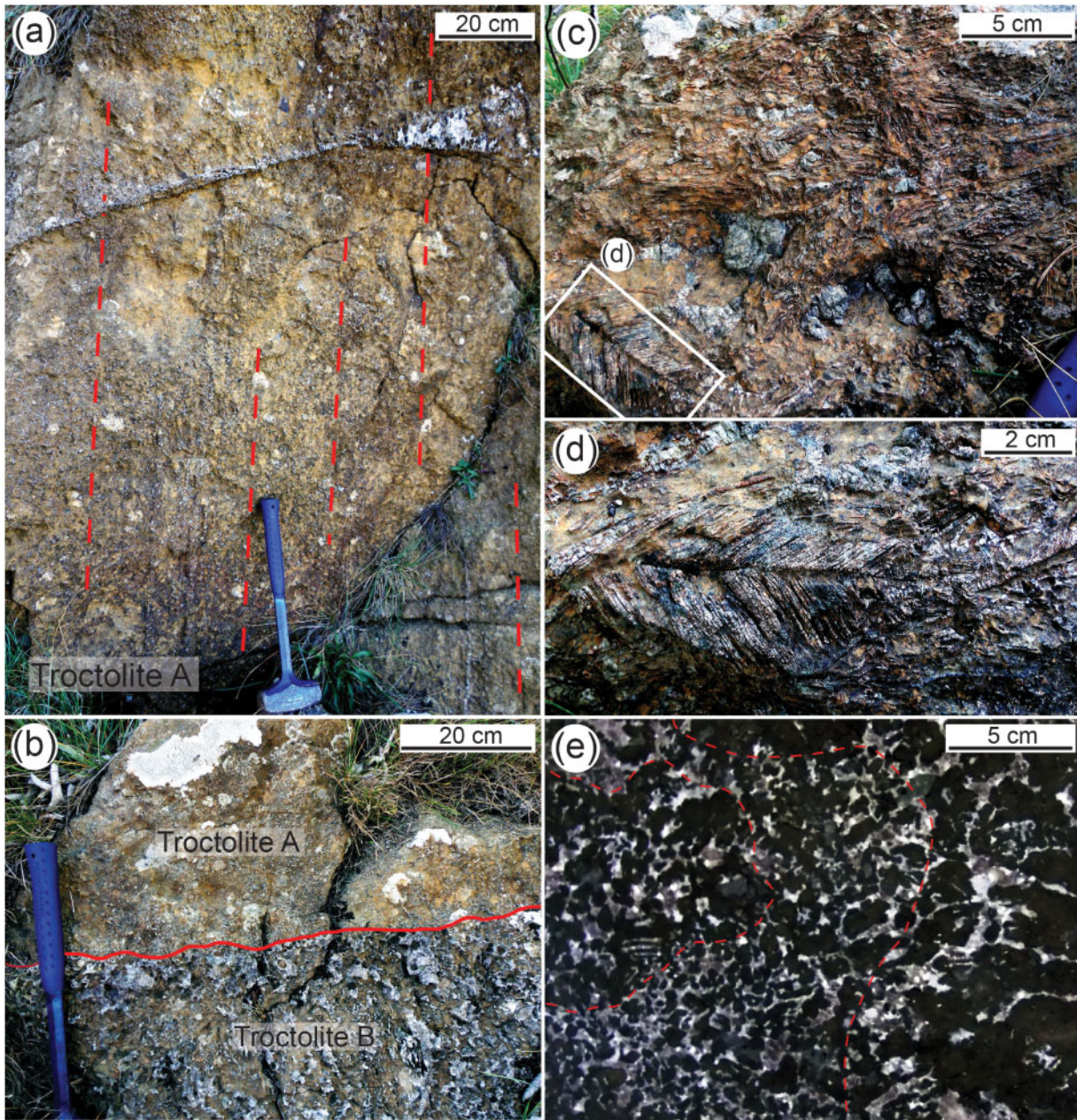


Fig. 3. Troctolite B field structures. (a) Troctolite B crosscutting the layering of plagioclase enrichment in Troctolite A (red dashed lines). (b) Irregular contact between Troctolite A and crosscutting Troctolite B. (c) Textural complexity within Troctolite B. The white rectangle indicates the location of (d). (d) Dendritic ‘fishbone’ olivine crystal. (e) Textural variability of olivine crystals at a centimetre-scale within Troctolite B. The dashed red line separates granular olivine domains from hopper and dendritic olivine domains.

Rampone & Borghini, 2008; Basch *et al.*, 2018) and in the Othris Massif (Dijkstra *et al.*, 2003).

Troctolite A

This has a hypidiomorphic texture and variable grain size, from centimetre-size anhedral to millimetre-size euhedral olivine crystals. Olivine occurs as either (1) fine-grained undeformed euhedral crystals embedded in interstitial to poikilitic plagioclase and clinopyroxene (Fig. 5a and b) or (2) coarse (up to centimetre-size)

deformed corroded grains, displaying kink bands (Fig. 5c and d). These two types of olivine are commonly found together, and in places fine-grained euhedral crystals of olivine embedded in poikilitic plagioclase or clinopyroxene show the same crystallographic orientation as a neighbouring coarse corroded grain of olivine (Fig. 5c).

Within Troctolite A, the textural variability includes small dunitic domains (olivine >90 vol. %; Fig. 6a–c), in which interstitial plagioclase surrounds millimetre-size to centimetre-size zones free of interstitial minerals, and

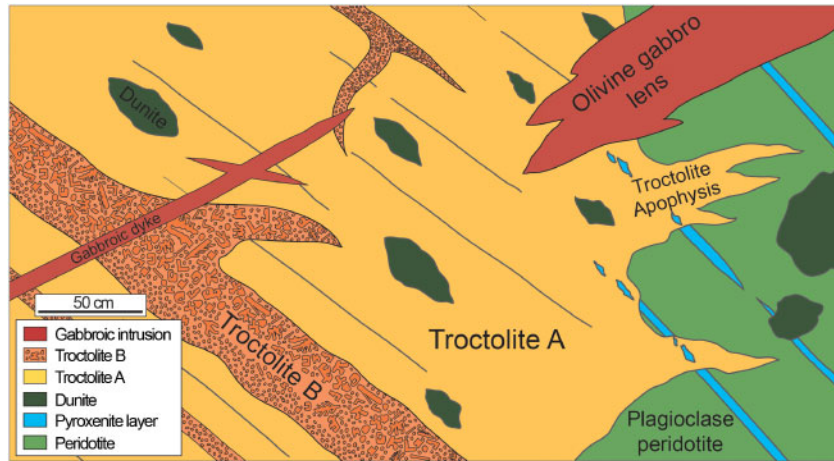


Fig. 4. Representative sketch of the crosscutting relationships observed in the field between the impregnated peridotites, the composite troctolitic body, and the gabbroic intrusions.

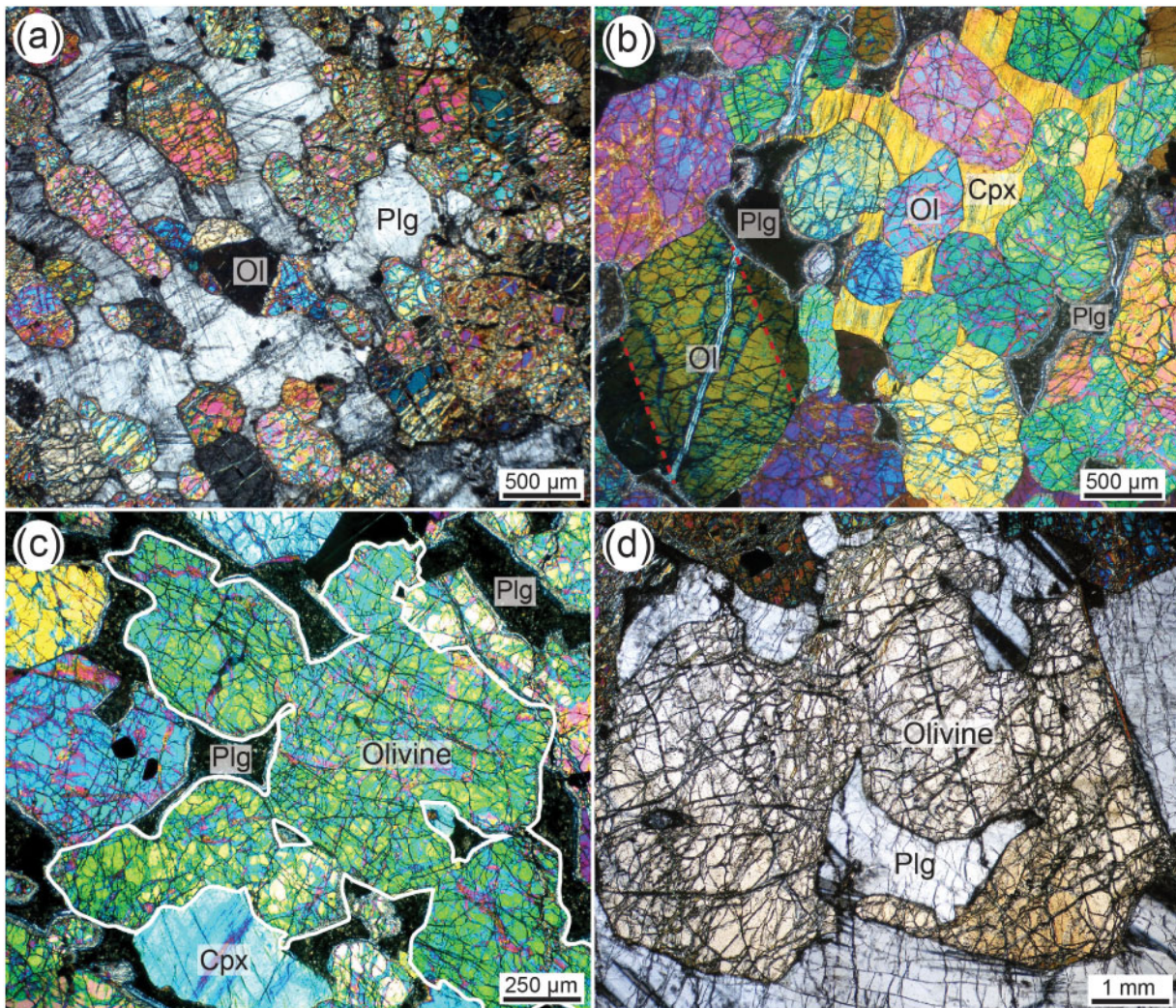


Fig. 5. Textural variability in Troctolite A. (a) Granular olivine matrix embedded in undeformed poikilitic plagioclase. (b) Granular olivine matrix embedded in poikilitic clinopyroxene. The largest olivine crystal shows the occurrence of kink bands, highlighted by the red dashed lines. Interstitial plagioclase has been replaced by low-grade alteration phases. (c) Corroded olivine grain prior to disruption into several smaller crystals. Interstitial plagioclase has been replaced by low-grade alteration phases. (d) Highly corroded centimetre-size olivine, embedded in poikilitic plagioclase.

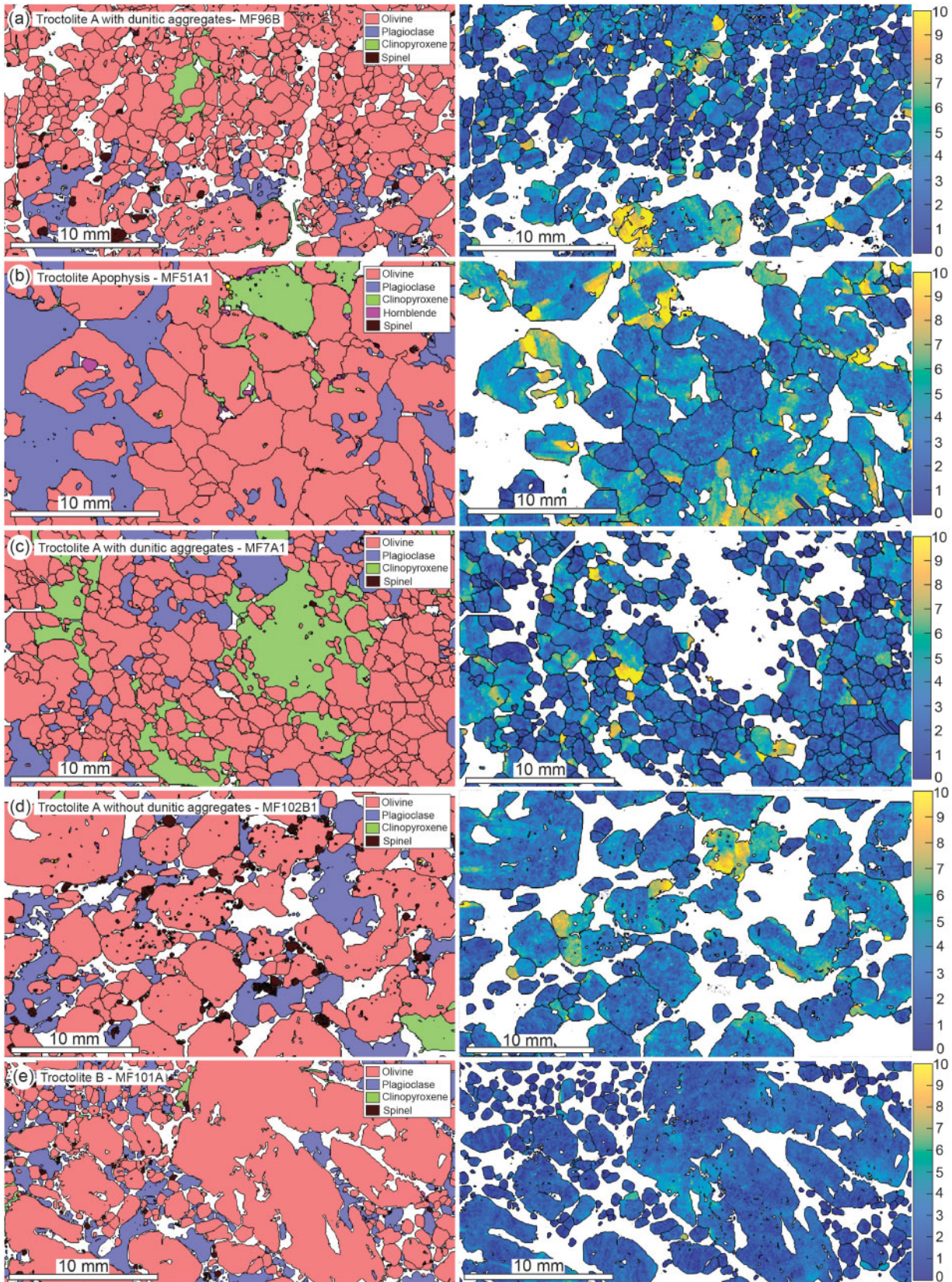


Fig. 6. EBSD phase (left column) and olivine misorientation (right column) maps showing the textural variability of the olivine matrix within the troctolitic body. (a) Troctolite A with dunitic aggregates MF96B; (b) troctolite apophysis MF51A1; (c) Troctolite A with dunitic aggregates MF7A1; (d) Troctolite A without dunitic aggregates MF102B1; (e) Troctolite B MF101A. White areas in the phase maps are non-indexed pixels, mostly corresponding to altered plagioclase.

plagioclase-rich domains (Fig. 6d) in which single olivines are entirely embedded in poikilitic plagioclase \pm clinopyroxene. Clinopyroxene, orthopyroxene, and amphibole are found as thin 'vermicular' crystals at the contact between olivine and poikilitic minerals and have been previously interpreted as post-cumulus crystallization of trapped melts (progressively evolving during late-stage closed-system crystallization; Borghini & Rampone, 2007; Borghini *et al.*, 2007). Spinel is found in the matrix, both associated with olivine as millimetre-size corroded grains (Fig. 6a, d) and with poikilitic plagioclase and clinopyroxene, as subhedral to euhedral smaller grains (\sim 100–200 μ m, Fig. 6d). Troctolite apophyses (part of Troctolite A) are very rich in coarse, deformed, corroded grains of olivine (Fig. 6b), and undeformed fine-grained olivine is rare.

Troctolite B

These pseudo-tabular bodies crosscut the host Troctolite A structures. They are characterized by lower olivine modal contents (from 45 to 60 vol. %; Table 1) than the host Troctolite A (from 55 to 97 vol. % olivine; Table 1). Moreover, Troctolite B shows extreme olivine textural variation, from millimetre-size euhedral crystals (Fig. 7a) to centimetre-size hopper (Fig. 7b), to decimetre-size dendritic and skeletal olivine (Figs 3b–e and 7c, d), all showing absent to weak deformation (Fig. 6e). In places, this textural variability leads to the formation of layering (Fig. 4), but all olivine morphologies can also be found together at the centimetre scale (Fig. 6e).

Gabbroic intrusions

These include gabbroic lenses, dykes and dykelets, mostly of olivine gabbro and minor troctolite, displaying hypidiomorphic textures and a fine- to coarse-grained olivine size. Subhedral plagioclase is the main rock-forming mineral (from 59 to 69 vol. % modal content of plagioclase; Table 1). Clinopyroxene is mostly found as large anhedral crystals including pre-existing euhedral plagioclase \pm olivine. Olivines (from 15 to 30 vol. % modal olivine; Table 1) are found both as euhedral grains included in plagioclase \pm clinopyroxene and as anhedral interstitial crystals in plagioclase–clinopyroxene–olivine aggregates, indicative of eutectic crystallization of the melt. These textural features in the gabbroic intrusions are indicative of an olivine–plagioclase–clinopyroxene crystallization sequence.

OLIVINE CRYSTALLOGRAPHIC PREFERRED ORIENTATIONS

In all studied samples of spinel lherzolite, plagioclase lherzolite and troctolite, a clear and representative olivine CPO could be quantified; however, because of the large grain size of the plagioclase and pyroxenes (Fig. 8; Bunge, 1982; Ben Ismail & Mainprice, 1998), no reliable

CPO of the interstitial minerals could be obtained at the thin-section scale. In the gabbroic intrusions, fine-grained euhedral plagioclase crystals also allow a representative quantification of the plagioclase CPO (Fig. 9).

Spinel lherzolites

Olivines in spinel lherzolites (ETR2, ETR4A, ETR4B in Table 1) are characterized by an axial-[100] CPO, with the [100] axis showing the strongest preferred orientation in the foliation plane, parallel to the lineation, [010] axis maximum oriented normal to the foliation plane, and [001] maximum within the foliation plane, normal to the lineation (Fig. 8). The J-index, representative of the fabric strength (e.g. Bunge, 1982; Ben Ismail & Mainprice, 1998; Mainprice *et al.*, 2014), ranges from 3.64 to 5.59 in spinel peridotites. Most natural peridotites show J-index values of olivine CPO between two and 20 (Tommasi *et al.*, 2000; Soustelle *et al.*, 2009).

Plagioclase lherzolites

Olivines in plagioclase lherzolites (P1A, P1B in Table 1) are characterized by a strong axial-[010] CPO (J-index = 5.5–7), with the strongest axis orientation being [010] normal to the foliation, and a girdle orientation of [100] and [001] within the foliation plane, showing a maximum parallel and normal to the lineation, respectively (Fig. 8).

Troctolite A with dunitic aggregates

In Troctolite A with dunitic aggregates (Fig. 6a–c; MF7A1, MF7A2, MF7C1, MF96A, MF96B in Table 1) and in the dunite pod associated with Troctolite A (MF104A in Table 1, Fig. 2c), all samples are characterized by a relatively weak (J-index = 2.04–3.83) but clear axial-[100] olivine CPO, with strongly oriented [100] axes within the foliation plane, [010] axes normal to the foliation, and a scatter of the [001] olivine axis orientations (Fig. 8). This olivine CPO is similar to that observed in the spinel lherzolites (Fig. 8).

Troctolite apophyses

These show a range of weak olivine CPOs from axial-[100] to axial-[010] (J-index = 1.86–2.1), similar to the CPO observed in spinel lherzolites and plagioclase lherzolites, respectively.

Troctolite A without dunitic aggregates

Troctolite A without dunitic aggregates (Fig. 6d; MF21, MF15, MF97, MF102B1 in Table 1) shows a very weak to random orientation of the [100] and [010] axes, and increased concentrations of the [001] olivine axis (J-index = 2.17–3.06).

Gabbroic intrusions

These (MF20II, MF24, MF11A1, MF99 in Table 1) show very weak olivine CPO (J-index = 1.21–1.83)

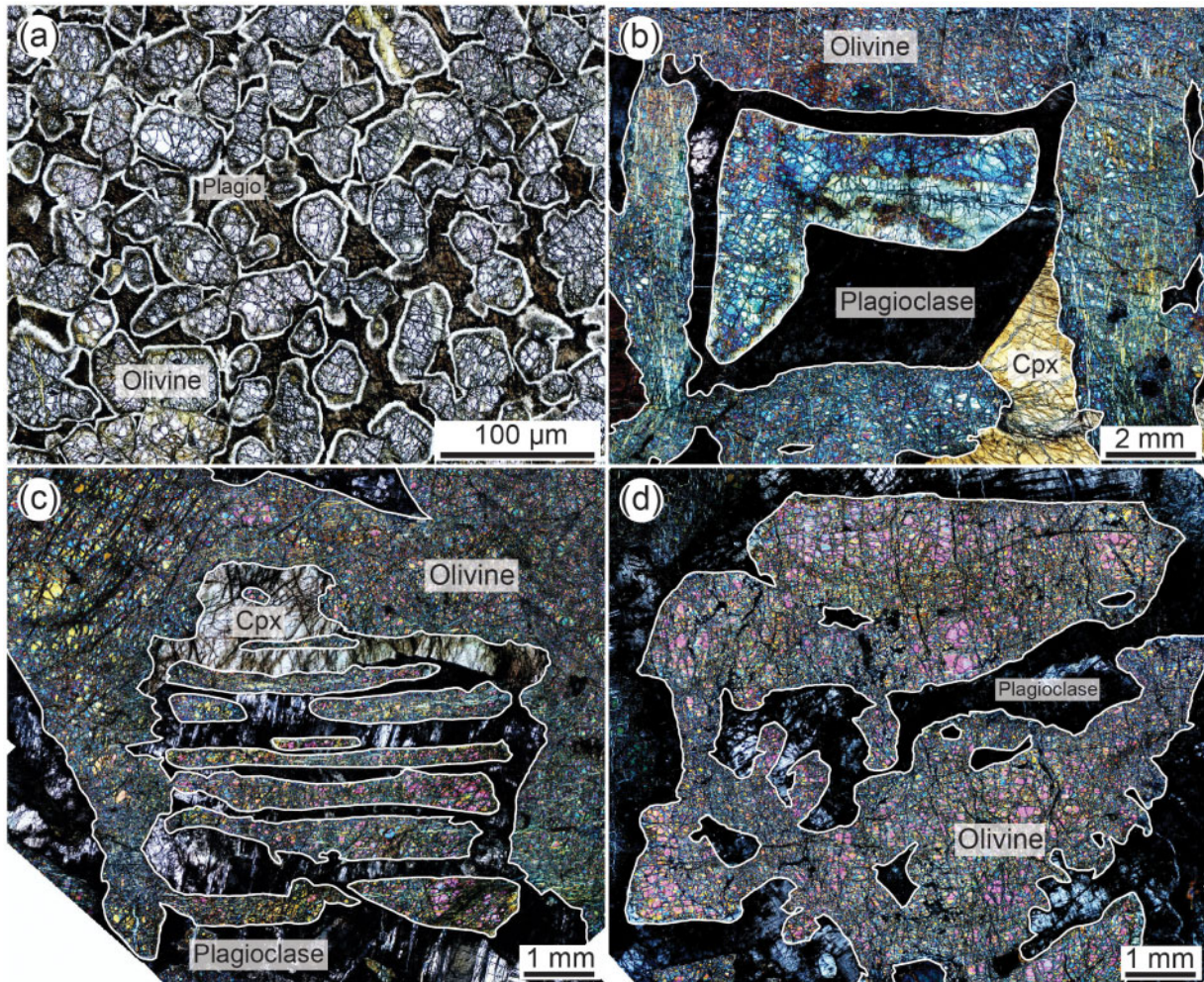


Fig. 7. Textural variability observed in the Troctolite B pseudo-tabular bodies. Plagioclase is partly to completely replaced by low-grade alteration phases. (a) Fine-grained granular undeformed olivines surrounded by a rim of chlorite; (b) partially corroded coarse hopper crystal of olivine, associated with poikilitic plagioclase and interstitial clinopyroxene; (c) coarse skeletal olivine showing the inner 'branches' of olivine, associated with interstitial plagioclase and clinopyroxene; (d) single coarse skeletal olivine associated with interstitial plagioclase.

characterized by [010] and [001] showing clear maxima normal and within the foliation plane, respectively (Fig. 9). Plagioclase shows a weak (J-index = 1.79–4.60) (010)[100] CPO characterized by a strong orientation of the [010] axis normal to the foliation plane (Fig. 9).

Troctolite B

Olivines in the granular part of Troctolite B (MF46A, MF94B in Table 1) are characterized by a strong orientation of the [010] and [001] axes normal and within the foliation plane, parallel to the lineation, respectively (Fig. 9). This (010)[001] olivine CPO is similar to that observed in the gabbroic intrusions (Benn & Allard, 1989; Jousselin *et al.*, 2012). The coarse poikilitic minerals in Troctolite B samples do not allow a reliable characterization of the plagioclase CPO at the thin-section scale (Fig. 9).

MAJOR ELEMENT MINERAL COMPOSITIONS

Representative major element compositions of olivine, clinopyroxene, plagioclase, orthopyroxene and spinel analyzed in spinel lherzolites, plagioclase lherzolites, Troctolites A, dunite, Troctolites B and gabbroic intrusions are reported in Tables 2–6 and the complete dataset is given in Supplementary Data Tables S1–S5. Overall our data show consistency with mineral compositions reported in previous studies of the Erro-Tobbio peridotites and associated gabbroic rocks (troctolitic body and gabbroic lenses and dykes) (Rampone *et al.*, 1993, 1998, 2004, 2005, 2016; Borghini & Rampone, 2007; Borghini *et al.*, 2007).

Olivine

Olivines in spinel lherzolites and plagioclase lherzolites have rather homogeneous high forsterite contents (Fo

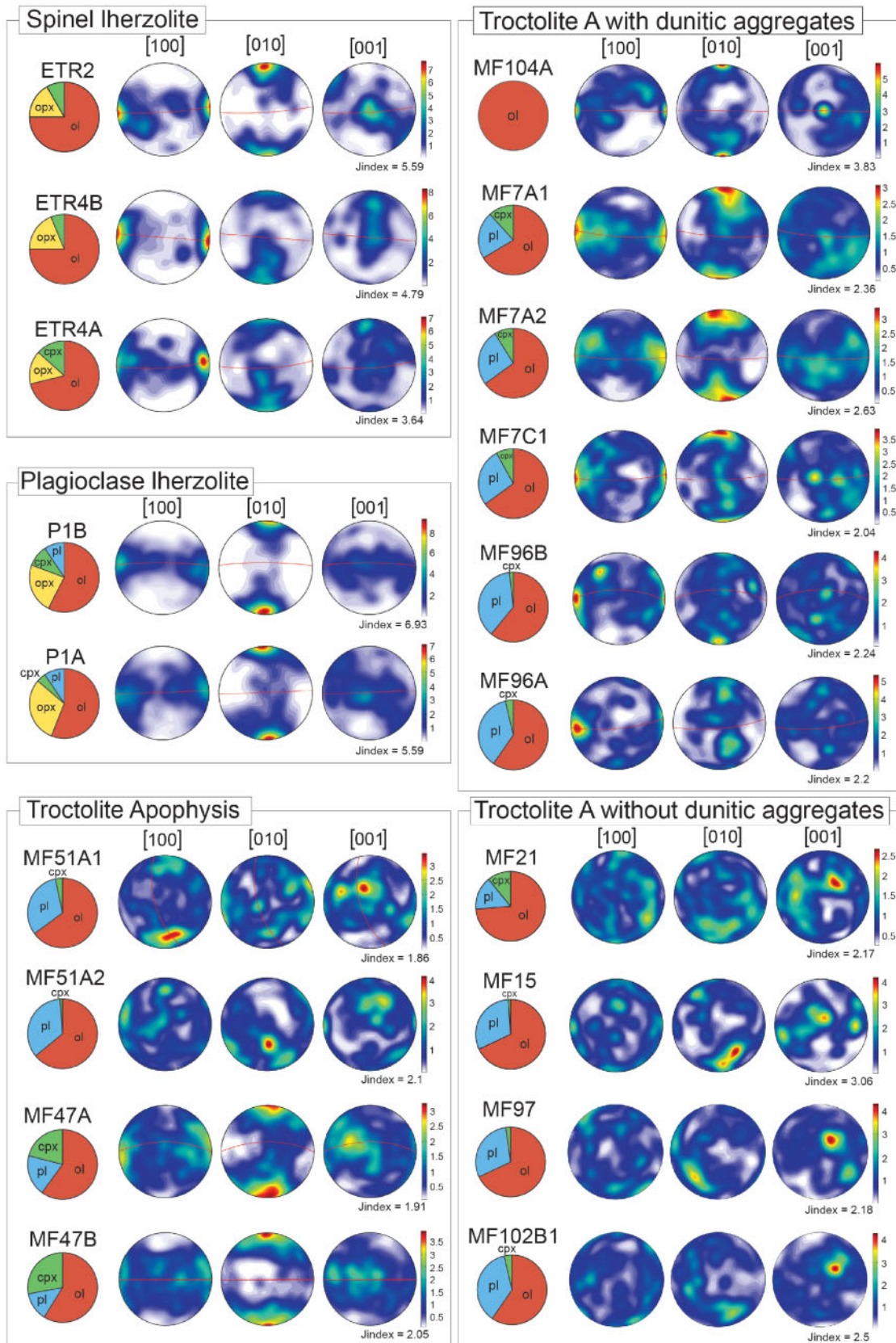


Fig. 8. Modal compositions and olivine crystallographic preferred orientation of spinel Iherzolite, plagioclase Iherzolite, troctolite apophysis and Troctolite A, with and without olivine aggregates. One-point-per-grain, equal-area, lower hemisphere stereographic projections. The colour bar is scaled to the maximum concentration of the three crystallographic axes. The foliation is indicated by the red line in oriented samples. J-index refers to the fabric strength.

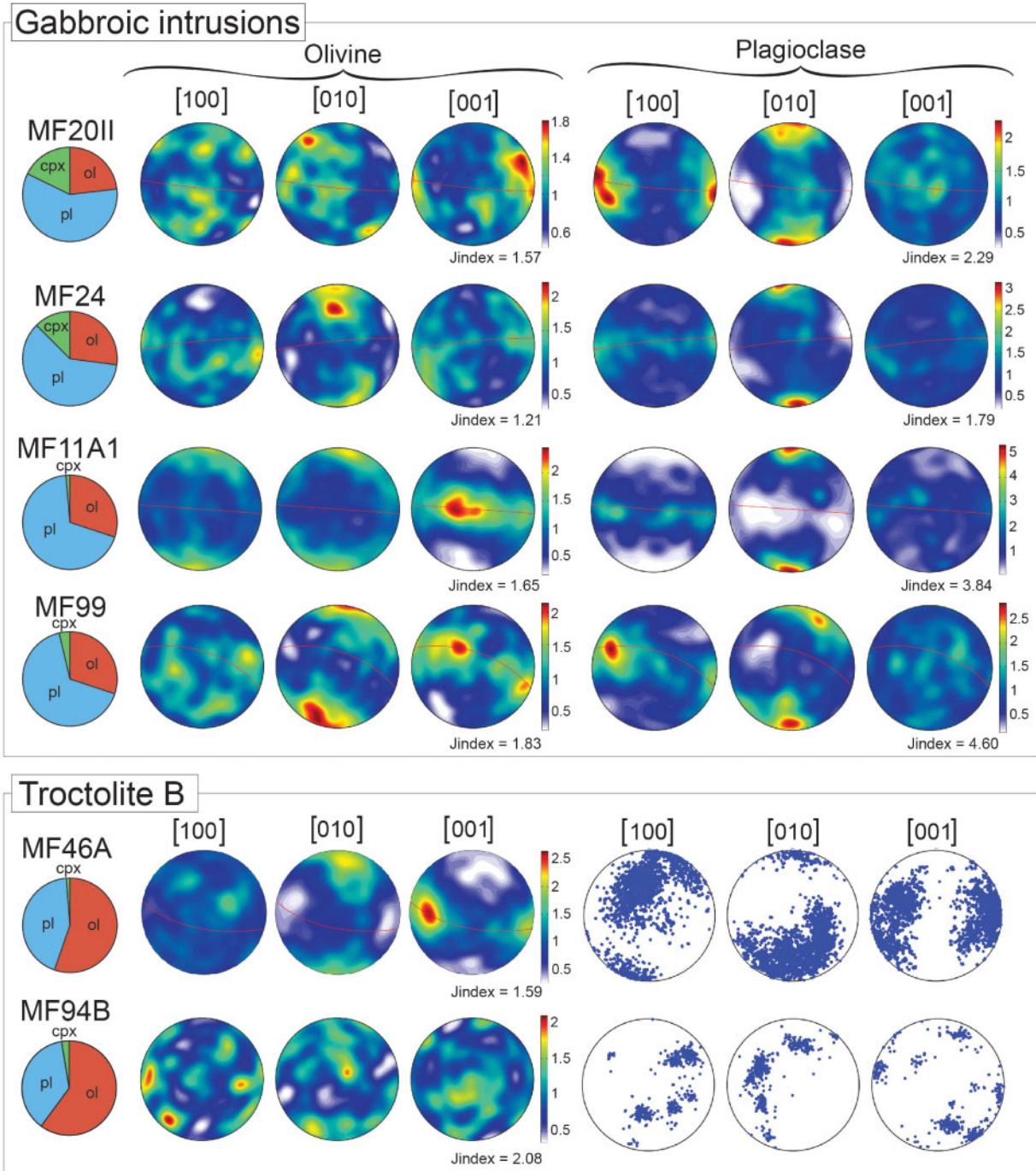


Fig. 9. Modal composition, olivine and plagioclase crystallographic preferred orientation of gabbroic intrusion and Troctolite B samples. One-point-per-grain equal-area, lower hemisphere stereographic projections. The colour bar is scaled to the maximum concentration of the three crystallographic axes. The foliation is indicated by the red line in oriented samples. J-index refers to the fabric strength.

= 89.5–90.5 mol % and Fo = 89.6–90.3 mol %, respectively; Fig. 10a) (Table 2). Olivines in Troctolites A and B have lower and more variable forsterite contents (Fo = 87.3–89.2 mol %). Within the troctolitic body, the main variations are observed between samples rather than within a single sample (Fig. 10a). No correlation is observed between the different olivine morphologies

described in Troctolite A or B and forsterite contents. Olivines within the dunite pod associated with Troctolite A show contents of forsterite = 88.2–89.1 mol % similar to olivines in Troctolite A (Fig. 10a). The wehr-lite apophysis MF47A (Table 1) has the lowest forsterite content analyzed in Troctolite A (Fo = 87.3–87.7 mol %). Gabbroic intrusions show a wide range of variation of

Table 2: Representative major element olivine composition

| | Spinel lherz. | Plagio. lherz. | Dunite | Troctolite A | | Troctolite apophysis | | Wehrlite apophysis | | Troctolite B | | Troct. gabbro | Troct. gabbro | Olivine gabbro | Olivine gabbro |
|--------------------------------|---------------|----------------|-----------|--------------|--------|----------------------|--------|--------------------|--------|--------------|--------|---------------|---------------|----------------|----------------|
| wt % | Corr.def. | Corr.def. | Corr.def. | Corr.def. | Granu. | Corr.def. | Granu. | Corr.def. | Granu. | Corr.def. | Granu. | Granu. | Granu. | Granu. | Granu. |
| SiO ₂ | 41.18 | 41.10 | 40.80 | 40.52 | 40.42 | 40.86 | 40.57 | 40.89 | 40.66 | 40.70 | 40.49 | 40.63 | 40.43 | 39.74 | 39.70 |
| TiO ₂ | 0.04 | 0.02 | 0.02 | 0.03 | b.d.l. | b.d.l. | 0.03 | 0.04 | 0.04 | 0.02 | b.d.l. | 0.01 | b.d.l. | b.d.l. | 0.03 |
| Al ₂ O ₃ | 0.01 | b.d.l. | 0.01 | b.d.l. | 0.02 | b.d.l. | 0.03 | b.d.l. | b.d.l. | b.d.l. | 0.04 | b.d.l. | 0.02 | b.d.l. | b.d.l. |
| Cr ₂ O ₃ | b.d.l. | b.d.l. | 0.02 | b.d.l. | b.d.l. | b.d.l. | b.d.l. | 0.01 | b.d.l. | 0.05 | b.d.l. | b.d.l. | b.d.l. | b.d.l. | b.d.l. |
| FeO | 9.64 | 10.05 | 11.29 | 11.65 | 11.75 | 11.31 | 11.29 | 11.81 | 11.96 | 11.61 | 11.52 | 11.11 | 13.38 | 16.11 | 17.57 |
| MgO | 49.47 | 48.99 | 47.65 | 48.05 | 48.02 | 48.01 | 48.21 | 47.33 | 47.33 | 47.90 | 48.05 | 48.22 | 46.49 | 44.35 | 43.16 |
| MnO | 0.11 | 0.16 | 0.21 | 0.18 | 0.15 | 0.23 | 0.15 | 0.20 | 0.22 | 0.18 | 0.17 | 0.17 | 0.21 | 0.27 | 0.33 |
| NiO | 0.37 | 0.43 | 0.28 | 0.30 | 0.28 | 0.33 | 0.29 | 0.27 | 0.31 | 0.31 | 0.32 | 0.33 | 0.26 | 0.21 | 0.14 |
| CaO | 0.03 | 0.06 | 0.09 | 0.06 | 0.04 | 0.07 | 0.05 | 0.05 | 0.04 | 0.08 | 0.02 | 0.04 | 0.01 | b.d.l. | 0.01 |
| Total | 100.85 | 100.83 | 100.37 | 100.81 | 100.69 | 100.84 | 100.63 | 100.60 | 100.58 | 100.86 | 100.63 | 100.54 | 100.80 | 100.68 | 100.96 |
| Mg# | 90.14 | 89.68 | 88.27 | 88.03 | 87.93 | 88.33 | 88.39 | 87.72 | 87.58 | 88.03 | 88.14 | 88.55 | 86.10 | 83.07 | 81.41 |

Mg# = Mg/(Mg + Fe); Spinel lherz., spinel lherzolite; Plagio. lherz., plagioclase lherzolite; Troct. gabbro, troctolitic gabbro; Corr.def., corroded-deformed; Granu., granular; b.d.l., below detection limit.

forsterite contents in olivine, from primitive compositions in the troctolitic intrusions (up to Fo = 89.2 mol %) to more evolved compositions in olivine gabbros (Fo = 81.3 mol %) (Table 1; Fig. 10b).

Clinopyroxene

Clinopyroxene cores in spinel lherzolites have high Mg-numbers (Mg# = 90.0–91.6 mol %), high Cr₂O₃ = 0.82–1.33 wt % and Al₂O₃ = 5.2–7.4 wt %, and low TiO₂ = 0.30–0.58 wt % (Table 3; Fig. 11a and b) contents. Impregnated plagioclase lherzolites show similar Mg-numbers (Mg# = 89.6–91.1 mol %) and TiO₂ = 0.4–0.53 wt % contents, higher Cr₂O₃ = 1.02–1.40 wt %, and lower Al₂O₃ = 2.83–5.27 wt % concentrations. Gabbroic intrusions exhibit clinopyroxene compositions consistent with olivine gabbros and troctolites from the South-West Indian Ridge (Dick *et al.*, 2002), with a positive correlation between Mg-number (Mg# = 83.5–90.8 mol %), Cr (Cr₂O₃ = 0.18–1.15 wt %), and Al (Al₂O₃ = 2.4–3.7 wt %), and a negative correlation with Ti (TiO₂ = 0.42–1.41 wt %) (Fig. 11a and b). Clinopyroxenes in Troctolite A (and associated dunite) and Troctolite B show high Cr (Cr₂O₃ = 1.17–1.67 wt %) and low Al (Al₂O₃ = 3.1–5.0 wt %) and Ti contents (TiO₂ = 0.12–0.92 wt %) (Fig. 11a and b).

Figure 11c and d shows the correlation between the clinopyroxene composition and its microstructural site. As previously documented by Borghini & Rampone (2007), clinopyroxenes in Troctolite A show progressively decreasing Cr₂O₃ (Cr₂O₃ = 0.78–1.67 wt %) and increasing TiO₂ (TiO₂ = 0.12–1.24 wt %) contents from core to rim to interstitial to vermicular microstructural sites, at constant Mg-number (Mg# = 87.7–91.0 mol %).

The Cr₂O₃, Al₂O₃ and TiO₂ compositional variability in clinopyroxene is well observed in major element core-rim profiles within single clinopyroxene grains (Fig. 12a–d). A progressive decrease in Cr₂O₃ (from 1.5 to 1.0 wt %) and Al₂O₃ (from 4 to 3 wt %), coupled with an increase in TiO₂ (from 0.4 to 1 wt %), is observed in the profiles, from the inner core towards the contact

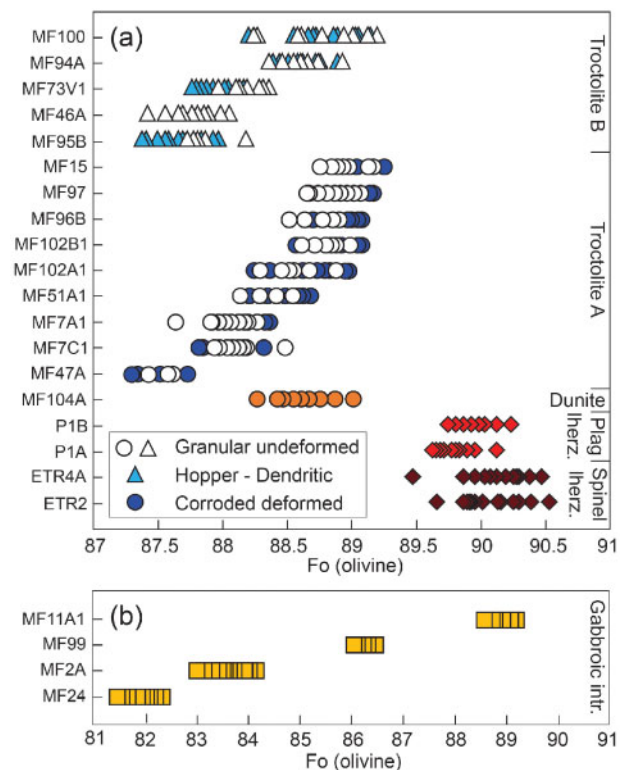


Fig. 10. Range of forsterite contents in olivines in (a) spinel lherzolite, plagioclase lherzolite, dunite, Troctolite A and Troctolite B and (b) gabbroic intrusions. Olivine morphology is divided into granular-undeformed and corroded-deformed within Troctolite A, and granular-undeformed and hopper-dendritic within Troctolite B.

between clinopyroxene and olivine (Rampone *et al.*, 2005). As documented by Borghini *et al.* (2007), the strong heterogeneity of Cr₂O₃, TiO₂ and Al₂O₃ in the clinopyroxenes of Troctolite A (Fig. 11c and d) is thus related to within-sample variations, clearly correlated with microstructural site. Geochemical variations in the profiles are observed from ~200 μm to the contact with the olivine (Fig. 12a–d).

Table 3: Representative major element clinopyroxene composition

| wt % | Spinel lherz. | | Plagio. lherz. | | Dunite | Troctolite A | | Troct. apophysis | | Wehrlite apophysis | Troctolite B | | Troct. gabbro | | Troct. gabbro | | Olivine gabbro | Olivine gabbro |
|--------------------------------|---------------|--------|----------------|-------|--------|--------------|-------|------------------|--------|--------------------|--------------|-------|---------------|-------|---------------|-------|----------------|----------------|
| | Core | Rim | Core | Rim | Core | Core | Rim | Core | Rim | Core | Core | Rim | Core | Core | Rim | Core | Core | |
| SiO ₂ | 51.24 | 51.70 | 50.98 | 52.05 | 52.31 | 51.70 | 52.74 | 51.05 | 52.62 | 51.45 | 52.14 | 51.46 | 51.76 | 51.72 | 51.92 | 52.70 | | |
| TiO ₂ | 0.36 | 0.40 | 0.50 | 0.98 | 0.40 | 0.92 | 0.58 | 1.00 | 0.35 | 0.64 | 1.02 | 0.92 | 0.73 | 0.75 | 0.89 | 0.73 | | |
| Al ₂ O ₃ | 6.59 | 4.48 | 4.87 | 2.96 | 3.61 | 3.34 | 3.05 | 2.99 | 3.51 | 3.62 | 3.23 | 3.28 | 3.35 | 3.21 | 2.80 | 2.51 | | |
| Cr ₂ O ₃ | 1.10 | 1.46 | 1.34 | 1.32 | 1.43 | 1.16 | 1.08 | 1.00 | 1.29 | 1.40 | 0.91 | 0.94 | 1.01 | 1.15 | 0.51 | 0.28 | | |
| FeO | 2.83 | 3.01 | 3.20 | 3.08 | 3.45 | 3.22 | 3.43 | 3.37 | 3.42 | 3.57 | 3.17 | 3.23 | 4.33 | 3.76 | 4.63 | 5.15 | | |
| MgO | 15.23 | 15.81 | 16.05 | 16.64 | 16.51 | 16.32 | 16.68 | 17.61 | 16.09 | 15.94 | 16.32 | 16.49 | 16.56 | 16.21 | 16.93 | 17.25 | | |
| MnO | 0.07 | 0.02 | 0.07 | 0.12 | 0.07 | 0.08 | 0.18 | 0.07 | 0.10 | 0.11 | 0.09 | 0.10 | 0.15 | 0.17 | 0.27 | 0.16 | | |
| NiO | 0.07 | 0.06 | 0.07 | 0.02 | b.d.l. | 0.04 | 0.04 | 0.06 | b.d.l. | 0.05 | 0.04 | 0.11 | 0.07 | 0.06 | b.d.l. | 0.03 | | |
| CaO | 22.25 | 22.86 | 22.29 | 21.74 | 20.90 | 22.03 | 21.47 | 21.26 | 22.17 | 21.60 | 22.49 | 21.85 | 20.61 | 21.61 | 22.65 | 20.30 | | |
| Na ₂ O | 0.71 | 0.38 | 0.26 | 0.65 | 0.62 | 0.56 | 0.05 | 0.58 | 0.55 | 0.64 | 0.62 | 0.46 | 0.46 | 0.60 | 0.35 | 0.45 | | |
| Total | 100.45 | 100.20 | 99.65 | 99.56 | 99.29 | 99.37 | 99.31 | 99.00 | 100.10 | 99.02 | 100.03 | 98.83 | 99.03 | 99.23 | 100.66 | 99.57 | | |
| Mg# | 90.56 | 90.35 | 89.94 | 90.59 | 89.51 | 90.03 | 89.66 | 90.30 | 89.34 | 88.84 | 90.17 | 90.10 | 87.21 | 88.48 | 86.70 | 85.65 | | |

Mg# = Mg/(Mg + Fe). Abbreviations as in Table 2.

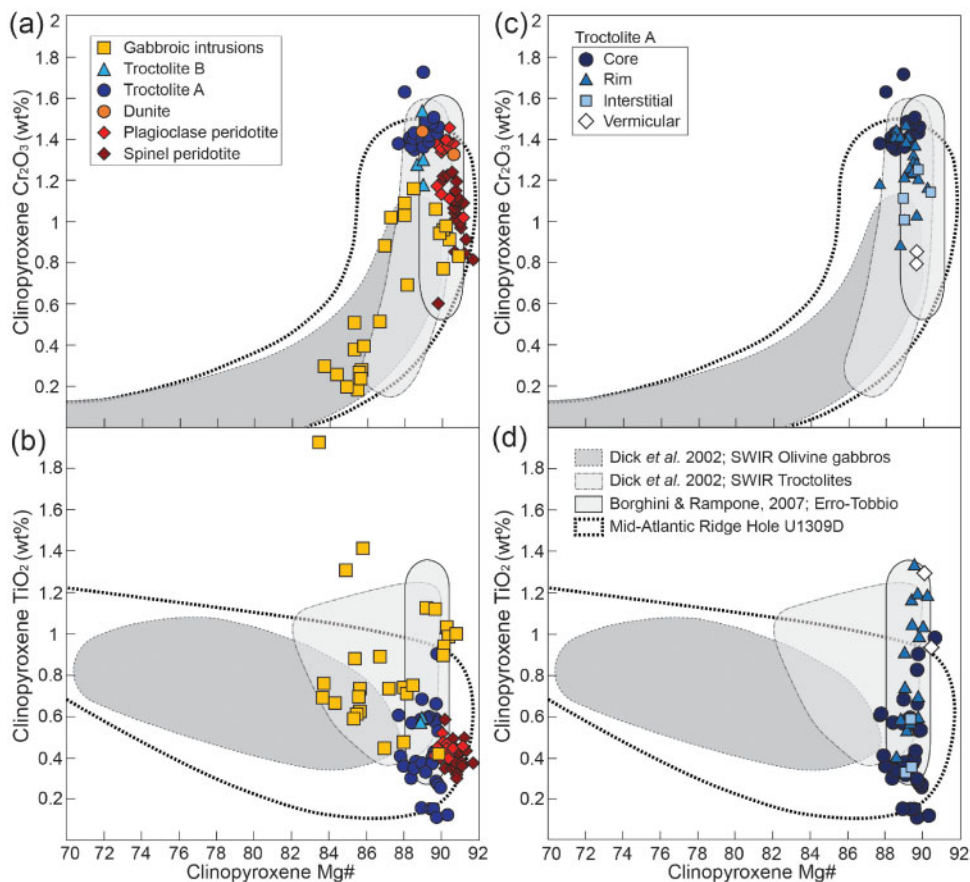


Fig. 11. Major element compositions of clinopyroxene cores (a, b) in all studied samples, plotted against the Mg-number [= Mg/(Mg + Fe)], and compositional variability with microstructural site (c, d) in Troctolite A. (a, c) Cr₂O₃ (wt %); (b, d) TiO₂ (wt %). Compositional fields represent the compositions of olivine gabbros and troctolites from the South-West Indian Ridge, after Dick *et al.* (2002), olivine-rich troctolites from Erro-Tobbio, after Borghini & Rampone (2007), and troctolites, olivine gabbros and gabbros from the Mid-Atlantic Ridge Hole U1309D, after Suhr *et al.* (2008), Drouin *et al.* (2009), Miller *et al.* (2009) and Ferrando *et al.* (2018).

Plagioclase

Plagioclases in Troctolite A (Table 4) are characterized by low and variable anorthite contents (An = 52.9–66.8 mol %) (Fig. 13). The same variability is observed in

Troctolite B, with anorthite contents of 55.1–66.1 mol %. Plagioclases in gabbroic intrusions show lower anorthite at 51.6–62.7 mol %. In all samples of Troctolite A and Troctolite B, a correlation is observed between the

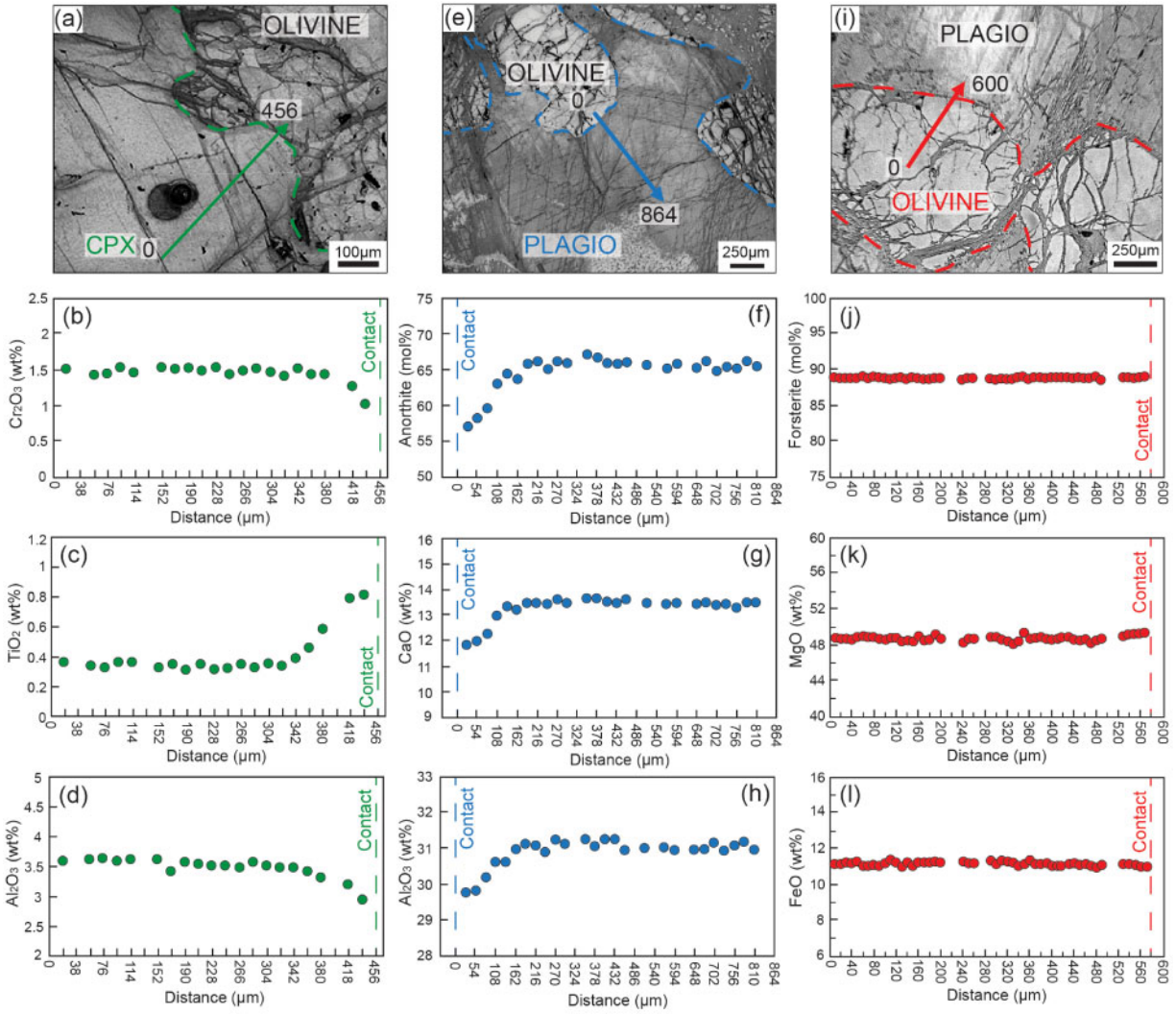


Fig. 12. Reflected light photomicrograph (a) and corresponding clinopyroxene major element profiles (b–d) for Troctolite A. Step size is 19 μm. (b) Cr₂O₃ (wt %); (c) TiO₂ (wt %); (d) Al₂O₃ (wt %). Total length of the profile is 456 μm. Reflected light photomicrograph (e) and corresponding plagioclase major element profiles (f–h) for Troctolite A. Step size is 54 μm. (f) Anorthite content (mol %); (g) CaO (wt %); (h) Al₂O₃ (wt %). Total length of the profile is 864 μm. Reflected light photomicrograph (i) and corresponding olivine major element profiles (j–l) for Troctolite A. Step size is 10 μm. (j) Forsterite content (mol %); (k) MgO (wt %); (l) FeO (wt %). Total length of the profile is 600 μm.

Table 4: Representative major element plagioclase composition

| wt % | Troctolite A | | Wehrlite apophysis | Troctolite apophysis | | Troctolite B | | Troct. gabbro | Troct. gabbro | | Olivine gabbro | | Olivine gabbro | |
|--------------------------------|--------------|--------|--------------------|----------------------|--------|--------------|--------|---------------|---------------|--------|----------------|--------|----------------|--------|
| | Core | Rim | Core | Core | Rim | Core | Rim | Core | Core | Rim | Core | Rim | Core | Rim |
| SiO ₂ | 52.22 | 54.11 | 52.74 | 52.08 | 54.76 | 51.21 | 52.95 | 52.08 | 53.41 | 53.73 | 53.53 | 55.03 | 54.53 | 54.05 |
| TiO ₂ | 0.10 | 0.10 | 0.02 | 0.21 | 0.09 | b.d.l. | 0.06 | 0.30 | 0.10 | 0.07 | b.d.l. | b.d.l. | 0.08 | 0.04 |
| Al ₂ O ₃ | 30.39 | 29.14 | 30.43 | 30.53 | 28.54 | 30.97 | 29.93 | 30.51 | 29.96 | 29.73 | 29.36 | 28.78 | 29.26 | 29.02 |
| Cr ₂ O ₃ | b.d.l. | b.d.l. | b.d.l. | b.d.l. | b.d.l. | 0.02 | 0.03 | b.d.l. | b.d.l. | b.d.l. | b.d.l. | b.d.l. | b.d.l. | b.d.l. |
| FeO | 0.16 | 0.15 | 0.20 | 0.02 | 0.02 | 0.23 | 0.17 | 0.30 | 0.33 | 0.20 | 0.35 | 0.27 | 0.27 | 0.30 |
| MgO | 0.03 | 0.01 | 0.05 | 0.01 | b.d.l. | b.d.l. | 0.02 | 0.05 | 0.04 | 0.07 | b.d.l. | b.d.l. | 0.05 | 0.02 |
| MnO | 0.02 | 0.03 | b.d.l. | 0.01 | b.d.l. | 0.01 | b.d.l. | 0.02 | 0.07 | b.d.l. | b.d.l. | b.d.l. | b.d.l. | b.d.l. |
| NiO | 0.03 | b.d.l. | 0.06 | b.d.l. | b.d.l. | b.d.l. | b.d.l. | b.d.l. | b.d.l. | b.d.l. | b.d.l. | b.d.l. | 0.02 | b.d.l. |
| CaO | 13.35 | 11.25 | 12.78 | 12.79 | 11.17 | 13.14 | 12.15 | 12.71 | 11.84 | 11.39 | 11.14 | 10.93 | 10.90 | 11.02 |
| Na ₂ O | 3.96 | 5.27 | 4.38 | 4.27 | 5.27 | 3.99 | 4.58 | 4.25 | 4.87 | 5.07 | 5.16 | 5.39 | 5.46 | 5.22 |
| K ₂ O | 0.03 | 0.04 | 0.04 | 0.02 | 0.03 | 0.02 | 0.04 | 0.02 | 0.02 | 0.03 | b.d.l. | b.d.l. | 0.02 | 0.03 |
| Total | 100.28 | 100.11 | 100.70 | 99.93 | 99.88 | 99.59 | 99.93 | 100.25 | 100.64 | 100.29 | 99.54 | 100.40 | 100.59 | 99.70 |
| An | 65.07 | 54.12 | 61.72 | 62.34 | 53.94 | 64.54 | 59.45 | 62.30 | 57.33 | 55.39 | 54.40 | 52.84 | 52.45 | 53.82 |

An = Ca/(Ca + Na). Abbreviations as in Table 2.

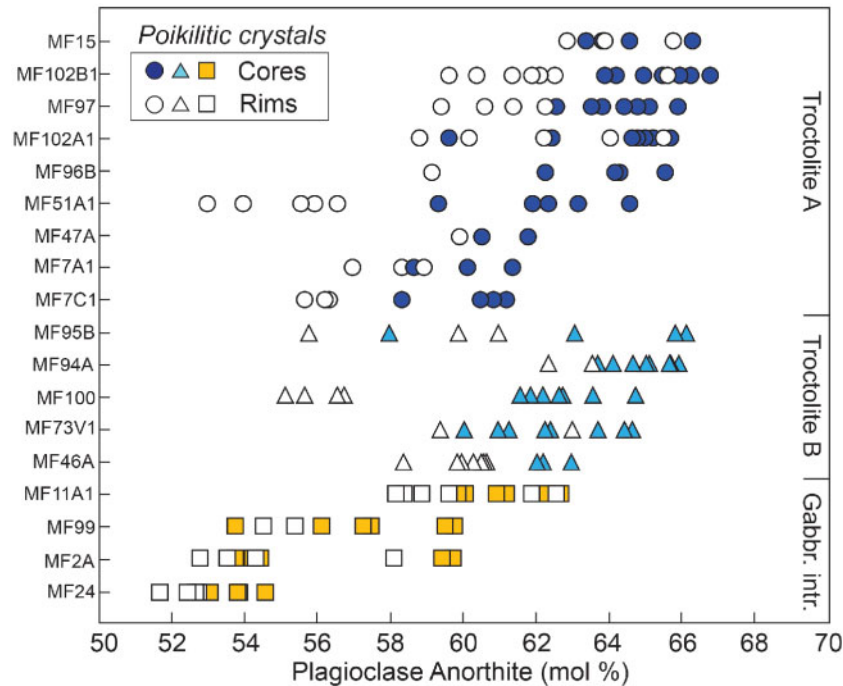


Fig. 13. Range of anorthite contents in plagioclase in Troctolite A, Troctolite B and gabbroic intrusions. Distinction has been made between cores (coloured symbols) and rims (white symbols) of coarse poikilitic plagioclase crystals.

microstructural site and the anorthite content of the analyzed plagioclase crystal. Thin interstitial crystals and rims of large grains systematically show lower anorthite contents than the plagioclase cores (Fig. 13), leading to a variation of anorthite content of up to 10 mol % within a single sample, in both Troctolites A and Troctolites B.

Again, these geochemical variations are well observed in major element profiles from core to rim of plagioclase crystals, at the contact with olivine. A progressive decrease in anorthite content (from 66 to 56 mol %), CaO (from 14 to 12 wt %), and Al₂O₃ (from 31 to 30 wt %) is observed in the profiles towards the rim and the contact with olivine (Fig. 12e–h), as previously documented by Borghini & Rampone (2007). Therefore, as observed for clinopyroxene, the strong compositional variation reported in single samples of Troctolite A and B (up to 10% anorthite content; Fig. 13) is not due to variations between different crystals, but to the zonation observed at the scale of a single grain (Fig. 12e–h). As documented in the clinopyroxene–olivine profiles, the chemical zoning in plagioclase is observed from ~200 μm to the contact with the olivine, irrespective of its textural type (coarse deformed corroded grain or small undeformed granular crystal).

In the gabbroic intrusions, no systematic zoning is observed in plagioclase, and the analyzed range of anorthite contents is mainly observed between samples (Fig. 13), with plagioclase in troctolitic dykes showing higher anorthite contents (MF11A1, MF99, An = 53.8–62.7 mol %; Table 1) than plagioclase within the olivine

gabbro dykes (MF2A, MF24, An = 51.6–54.6 mol %; Table 1).

Orthopyroxene

Orthopyroxenes (Table 5) analyzed in evolved gabbroic intrusions have lower Mg-numbers (Mg# = 84–53 mol %) than the homogeneous orthopyroxene compositions analyzed in the spinel and plagioclase lherzolites (Mg# = 89–64–90–54 mol %).

Spinel

Spinel in spinel lherzolites (Table 6) exhibit high Mg-numbers (Mg# = 66.9–72.8 mol %), low Cr-numbers (Cr# = 14.2–18.6 mol %), and very low TiO₂ contents (0.02–0.16 wt %), similar to spinel compositions in plagioclase-free peridotites from the South-West Indian Ridge (Seyler *et al.*, 2003). In the gabbroic intrusions, the spinels have low Mg-numbers (Mg# = 25.2–36.1 mol %), and high Cr-numbers (Cr# = 63.6–69.0 mol %) and TiO₂ (1.22–1.49 wt %).

In Troctolite A, dunite and Troctolite B, spinels show Mg-numbers (Mg# = 19.2–55.6 mol %) and Cr-numbers (Cr# = 40.5–64.5 mol %) intermediate between spinel compositions in the spinel lherzolites and the gabbroic intrusions, and a negative correlation is observed between the Mg-number and the Cr-number, consistent with spinel compositions in troctolites from the Mid-Atlantic Ridge (Miller *et al.*, 2009). Some spinels in Troctolite A and Troctolite B, and most of them in the dunite show strong enrichments in TiO₂ (0.79–3.27 wt %), up to twice the TiO₂ concentrations analyzed in

gabbroic intrusions. The negative correlation between Mg-number and TiO₂ concentrations in spinel analyzed in Troctolite A, associated dunites and Troctolite B is consistent with the trend reported for spinels analyzed in troctolites from the Mid-Atlantic Ridge (Miller *et al.*, 2009).

Element partitioning between mineral pairs

Figure 14a shows the Mg–Fe partitioning between olivine and clinopyroxene in all studied lithotypes. Overall, the studied samples show a positive correlation between forsterite contents in olivine (from Fo = 81.3 mol % in gabbroic intrusions to Fo = 90.5 mol % in spinel lherzolites) and Mg-number in clinopyroxene (from Mg# = 83.5 mol % in gabbroic intrusions to Mg# = 91.6 mol % in spinel lherzolite). This correlation is consistent with the Mg–Fe equilibrium lines calculated between olivine and clinopyroxene by Lissenberg & Dick (2008) [$Kd_{ol/cpx}(Fe\#) = 1.30$] (Fig. 14a). Pairs of olivine and clinopyroxene cores in Troctolite A, dunite, and Troctolite B show compositions (Fo = 87.3–89.2 mol %, Mg# = 87.7–91 mol %) that are intermediate between those of the Mg-rich pairs analyzed in spinel and plagioclase lherzolites (Fo = 89.5–90.5 mol %, Mg# = 89.6–

91.6 mol %) and the most evolved compositions in the gabbroic intrusions (Fo = 81.3–89.2 mol %, Mg# = 83.5–90.8 mol %).

Figure 14b shows anorthite and forsterite contents (mol %) in plagioclase–olivine core pairs in Troctolite A, Troctolite B and the gabbroic intrusions. Within the troctolitic body, plagioclase–olivine pairs show significant variations in anorthite content of plagioclase cores (An = 58.4–66.8 mol %) at constant forsterite composition in associated olivines (87.3–89.2 mol %), similar to what was reported at the easternmost South-West Indian Ridge (61–67°E) (Paquet *et al.*, 2016). By contrast, the gabbroic intrusions define a trend of evolution characterized by a positive correlation between anorthite content in plagioclase cores and forsterite content in olivine (from An_{51.6}–Fo_{81.3} to An_{62.7}–Fo_{89.2}). This trend in the gabbroic intrusions shows a similar slope to the compositional arrays defined by olivine gabbros in the oceanic lower crust from the South-West Indian Ridge (Hole 735B: Dick *et al.*, 2002), Mid-Atlantic Ridge (Ross & Elthon, 1997; Lissenberg & Dick, 2008; Suhr *et al.*, 2008; Drouin *et al.*, 2009; Miller *et al.*, 2009), and Pineto ophiolite (Sanfilippo & Tribuzio, 2013), but shifted towards higher forsterite contents of olivine (Fig. 14b).

Clinopyroxene Mg-number (mol %) shows similar correlations with plagioclase anorthite (mol %) content (Fig. 14c), with a relatively constant Mg-number in Troctolite A and Troctolite B (Mg# = 87.7–91.0 mol %) at varying anorthite content (An = 55.1–67.0 mol %), similar to mineral compositions analyzed at the easternmost South-West Indian Ridge (61–67°E) (Paquet *et al.*, 2016). The gabbroic intrusions show a positive correlation between Mg-number in clinopyroxene and anorthite content in plagioclase (from An_{51.6}–Mg#_{83.7} to An_{62.7}–Mg#_{90.1}). The slope defined by the anorthite–Mg-number (cpx) covariation in the gabbroic intrusions is consistent with the trends documented in the oceanic gabbro suites at the Mid-Atlantic Ridge (Ross & Elthon, 1997; Lissenberg & Dick, 2008; Suhr *et al.*, 2008; Drouin *et al.*, 2009; Miller *et al.*, 2009; Ferrando *et al.*, 2018), South-West Indian Ridge (Dick *et al.*, 2002), and in the

Table 5: Representative major element orthopyroxene composition

| wt % | Spinel lherzolite | Plagioclase lherzolite | | Olivine gabbro Core |
|--------------------------------|-------------------|------------------------|--------|---------------------|
| | Core | Core | Rim | |
| SiO ₂ | 55.40 | 56.18 | 55.43 | 54.83 |
| TiO ₂ | 0.10 | 0.24 | 0.21 | 0.28 |
| Al ₂ O ₃ | 4.88 | 2.39 | 2.63 | 2.30 |
| Cr ₂ O ₃ | 0.73 | 0.65 | 0.82 | 0.19 |
| FeO | 6.26 | 6.27 | 5.95 | 10.05 |
| MgO | 32.10 | 32.64 | 31.69 | 30.82 |
| MnO | 0.15 | 0.08 | 0.14 | 0.22 |
| NiO | 0.08 | 0.07 | 0.10 | b.d.l. |
| CaO | 0.85 | 1.52 | 3.22 | 1.33 |
| Na ₂ O | 0.03 | 0.01 | 0.03 | b.d.l. |
| Total | 100.57 | 100.05 | 100.22 | 100.02 |
| Mg# | 90.14 | 90.27 | 90.47 | 84.53 |

$$\text{Mg\#} = \text{Mg}/(\text{Mg} + \text{Fe}).$$

Table 6: Representative major element spinel composition

| wt % | Spinel lherz. | Dunite | Troct. A | Troct. apo. | Troct. B | Troct. gabbro |
|--------------------------------|---------------|--------|----------|-------------|----------|---------------|
| SiO ₂ | b.d.l. | 0.03 | 0.02 | b.d.l. | 0.05 | b.d.l. |
| TiO ₂ | 0.07 | 2.91 | 1.66 | 1.27 | 2.01 | 1.39 |
| Al ₂ O ₃ | 53.68 | 15.19 | 17.90 | 16.33 | 21.41 | 12.89 |
| Cr ₂ O ₃ | 14.82 | 38.02 | 35.94 | 38.79 | 35.93 | 42.77 |
| Fe ₂ O ₃ | 1.03 | 11.65 | b.d.l. | b.d.l. | 7.83 | b.d.l. |
| FeO | 12.78 | 23.60 | 36.35 | 35.93 | 23.20 | 35.89 |
| MnO | b.d.l. | b.d.l. | 0.23 | 0.03 | b.d.l. | 0.38 |
| NiO | b.d.l. | b.d.l. | 0.27 | 0.02 | b.d.l. | 0.12 |
| MgO | 18.31 | 8.76 | 6.82 | 7.29 | 8.93 | 6.79 |
| CaO | b.d.l. | 0.01 | 0.03 | b.d.l. | 0.01 | b.d.l. |
| Total | 100.69 | 100.17 | 99.23 | 99.67 | 99.41 | 100.29 |
| Cr# | 0.16 | 0.63 | 0.57 | 0.61 | 0.53 | 0.69 |
| Mg# | 0.70 | 0.31 | 0.25 | 0.27 | 0.34 | 0.25 |

$$\text{Mg\#} = \text{Mg}/(\text{Fe} + \text{Mg}); \text{Cr\#} = \text{Cr}/(\text{Cr} + \text{Al} + \text{Fe}^{3+}). \text{ Abbreviations as in Table 2.}$$

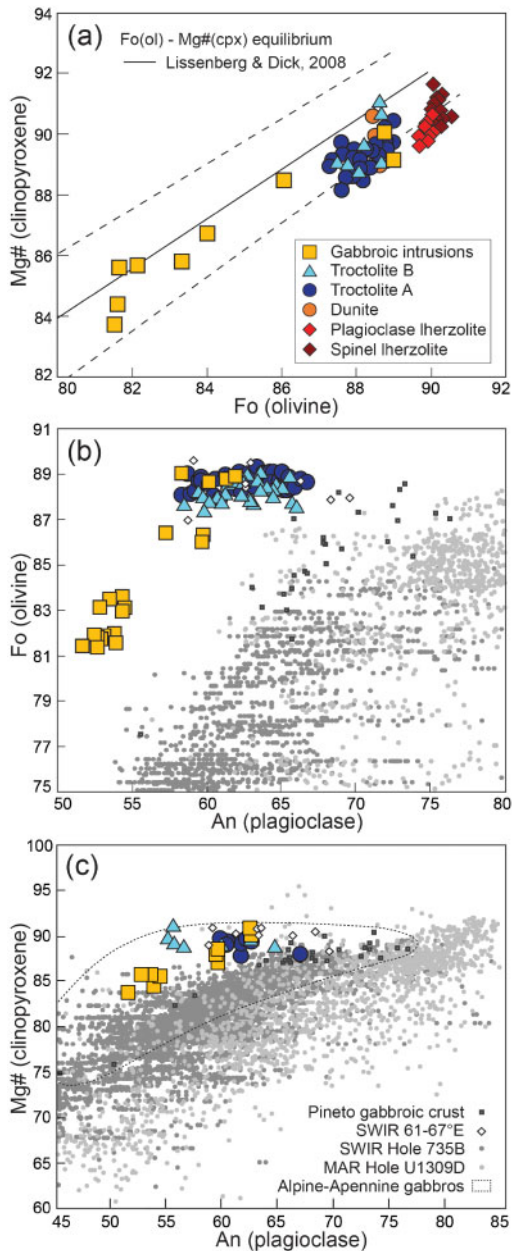


Fig. 14. (a) Olivine–clinopyroxene cores Mg# [= Mg/(Mg + Fe) (mol %)] correlation in the studied samples, compared with theoretical Fe–Mg equilibrium between olivine and clinopyroxene, after Lissenberg & Dick (2008). The dashed lines represent the calculated olivine–clinopyroxene equilibrium line assuming an uncertainty of ± 0.02 on the mineral–melt partition coefficients. (b) Anorthite content (mol %) in plagioclase cores vs forsterite content (mol %) in olivine cores in olivine–plagioclase pairs from the studied Troctolite A, Troctolite B and gabbroic intrusions. (c) Anorthite content (mol %) in plagioclase cores vs Mg-number (mol %) in clinopyroxene cores in plagioclase–clinopyroxene pairs from the studied Troctolite A, Troctolite B and gabbroic intrusions. Compositional trends and fields represent olivine–plagioclase and olivine–clinopyroxene pairs in olivine gabbros and troctolites from the South-West Indian Ridge (Hole 735B: Dick *et al.*, 2002; 61–67°: Paquet *et al.*, 2016), the Mid-Atlantic Ridge Hole U1309D (Ross & Elthon, 1997; Lissenberg & Dick, 2008; Suhr *et al.*, 2008; Drouin *et al.*, 2009; Miller *et al.*, 2009), the Pineto gabbroic crust (Sanfilippo & Tribuzio, 2013), and the Alpine–Apennine ophiolites (Hébert *et al.*, 1989; Tribuzio *et al.*, 1999; Montanini *et al.*, 2008; Sanfilippo & Tribuzio, 2013).

Pineto gabbroic crust (Sanfilippo & Tribuzio, 2013), but shifted towards higher Mg-number values of clinopyroxene (Fig. 14c). Also shown is the compositional field of Alpine–Apennine troctolites, olivine gabbros and gabbros (Hébert *et al.*, 1989; Tribuzio *et al.*, 1999; Montanini *et al.*, 2008; Sanfilippo & Tribuzio, 2013), characterized by lower anorthite contents in plagioclase at a given Mg-number in clinopyroxene, compared with oceanic gabbroic series [Fig. 14c; South-West Indian Ridge (SWIR) Hole 735B: Dick *et al.*, 2002; Mid-Atlantic Ridge (MAR) Hole U1309D: Ross & Elthon, 1997; Lissenberg & Dick, 2008; Suhr *et al.*, 2008; Drouin *et al.*, 2009; Miller *et al.*, 2009; Ferrando *et al.*, 2018].

DISCUSSION

Replacive origin of Troctolite A

As documented in previous studies and herein, the Erro–Tobbio troctolitic body crosscuts the host impregnated plagioclase lherzolites and associated pyroxenite banding (Fig. 4; Borghini & Rampone, 2007; Borghini *et al.*, 2007; Rampone *et al.*, 2016), includes dunite pods, and develops wehrlite and troctolite apophyses into the mantle plagioclase lherzolites (Fig. 2a). Troctolite A shows a strong textural complexity with the occurrence of two distinct types of olivine within individual samples (Fig. 6a–d); that is, millimetre-size undeformed granular olivine grains (Fig. 5a and b) and coarse (up to centimetre-size) deformed and corroded crystals (Fig. 5c and d). As inferred for oceanic settings during the formation of olivine-rich troctolites (Suhr *et al.*, 2008; Drouin *et al.*, 2010), Rampone *et al.* (2016) interpreted the textural complexity of the Erro–Tobbio troctolites as the result of melt–rock interactions leading to the dissolution of the olivine matrix and crystallization of interstitial plagioclase. Although they were not able to distinguish two olivine generations in a specific troctolite sample, they inferred that the millimetre-size undeformed granular olivine grains could represent a second generation of ‘olivine 2’, whether of magmatic origin or representing disrupted coarse olivine grains. Detailed EBSD analysis (size, shape, misorientation; Fig. 6) allows us to interpret the coarse deformed and corroded olivine as the pre-existing, possibly mantle relict ‘olivine 1’. The occurrence of coarse corroded grains almost disrupted into several granular olivines (Fig. 5c) suggests that most of the small undeformed olivine grains were formed after extensive corrosion and disruption of the coarse pre-existing olivines. This process of textural evolution of the olivine matrix, during progressive melt–rock interaction and replacive formation of olivine-rich troctolites, has been previously inferred in oceanic settings (Suhr *et al.*, 2008; Drouin *et al.*, 2010; Ferrando *et al.*, 2018) and recently demonstrated in an ophiolitic setting at the Mt. Maggiore peridotitic body (Basch *et al.*, 2018).

At the scale of the sample, Troctolite A is also characterized by variations in the texture of the olivine matrix (taken as a whole, olivine 1 + olivine 2), between

samples characterized by plagioclase-free dunitic aggregates surrounded by interstitial phases (Fig. 6a–c), and disaggregated samples where single olivines are completely embedded in poikilitic plagioclase (Fig. 6d). This textural variability is well correlated with a change in olivine CPO. The olivine matrix of Troctolite A, characterized by plagioclase-free dunitic aggregates, shows an axial-[100] fabric (Fig. 8), similar to that of the spinel lherzolites and dunite pods. This axial-[100] CPO is typically reported in natural peridotites deformed under asthenospheric conditions (e.g. Tommasi *et al.*, 2000; Le Roux *et al.*, 2008; Soustelle *et al.*, 2009), and indicates that plastic deformation was related to dislocation creep with joint activation of the (010)[100] and (001)[100] slip systems, the most easily activated at high-temperature conditions (1100–1200°C) (Ben Ismail & Mainprice, 1998; Tommasi *et al.*, 2000; Karato *et al.*, 2008; Drouin *et al.*, 2010; Higgie & Tommasi, 2012). The samples characterized by a disaggregated olivine matrix, embedded in poikilitic plagioclase, show scattered orientations of [100] and [010] olivine axes, and a stronger concentration of the [001] axis (Fig. 8). Such olivine CPOs have been previously reported in zones of melt accumulation in the Oman Moho Transition Zone (Ceuleneer & Rabinowicz, 1992; Boudier & Nicolas, 1995; Joussetin *et al.*, 1998; Dijkstra *et al.*, 2002; Higgie & Tommasi, 2012) and during the replacive formation of olivine-rich troctolites at the Atlantis Massif (Drouin *et al.*, 2010). It has been interpreted as a loss of cohesion of the solid matrix during impregnation at high melt/rock ratios (20–40% melt fraction; Rosenberg & Handy, 2005). Melt–rock interaction microstructures, indicating the corrosion of the pre-existing olivine matrix, together with the preservation of dunitic pods within the host Troctolite A (Figs 2d and 4) and the correlation between the observed texture of the olivine matrix and its CPO (Fig. 8), suggest a replacive formation of Troctolites A. We infer that they formed from a mantle dunite protolith (itself preserving the mantle precursor axial-[100] CPO), after reactive percolation of a MORB-type melt at variable melt/rock ratios (Fig. 15). The disaggregation of the olivine matrix associated with the loss of the olivine axial-[100] CPO are indicative of high instantaneous melt/rock ratios (>20–40%; Rosenberg & Handy, 2005), whereas the samples preserving the mantle olivine CPO indicate a reactive percolation at lower melt/rock ratios (Fig. 15). Texture and CPO analyses, together with the occurrence of preserved dunitic pods within Troctolite A, thus indicate that Troctolite A is probably the replacive product of reactive percolation and impregnation of a pristine dunitic matrix by melts crystallizing plagioclase and minor clinopyroxene.

Peculiar geochemical compositional trends for the rock-forming minerals, not consistent with a simple fractional crystallization process, support the replacive origin of Troctolites A. Despite strong variations in olivine modal compositions (from 55 vol. % in troctolites to 97 vol. % in dunitic pods), olivines and clinopyroxenes

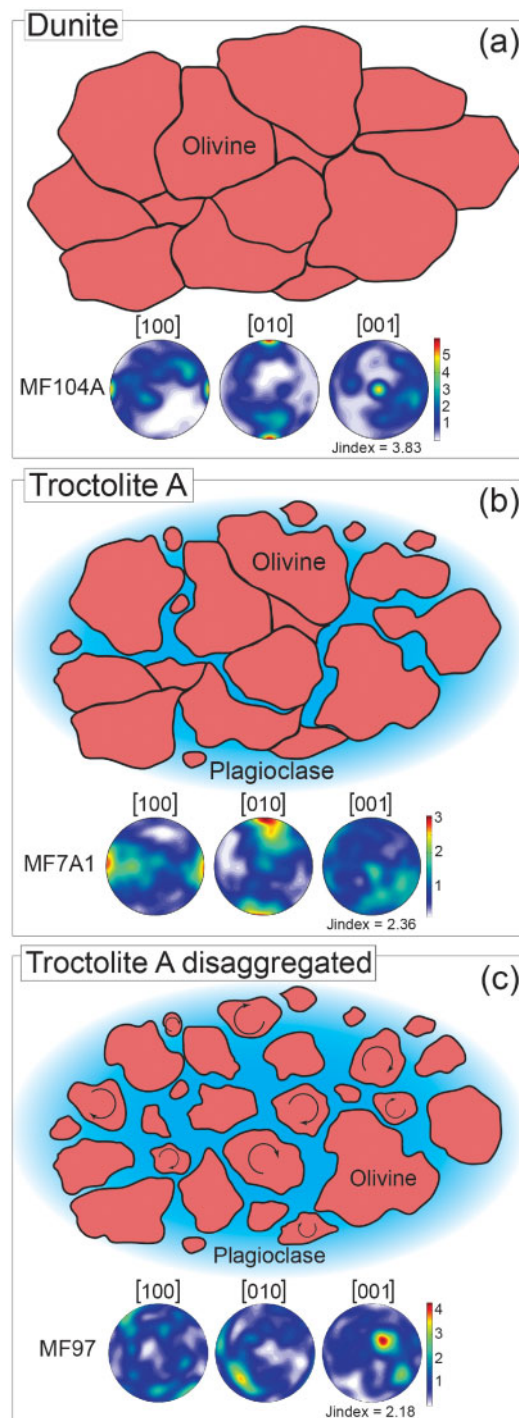


Fig. 15. Interpretative sketches of the evolution of the olivine textures and associated CPOs during progressive olivine-dissolving, plagioclase-crystallizing melt–rock interaction and replacive formation of Troctolite A. (a) Coarse-grained dunite protolith showing an axial [100] olivine CPO; (b) Troctolite A impregnated at a low melt–rock ratio, and thus preserving dunitic aggregates and axial [100] olivine CPO; (c) disaggregated Troctolite A, impregnated at high instantaneous melt–rock ratios. The arrows within small olivine grains represent the loss of cohesion of the solid matrix leading to the free rotation of the grains and randomization of the olivine CPO. CPO represented as one-point-per-grain equal-area, lower hemisphere stereographic projections. The colour bar is scaled to the maximum concentration of the three crystallographic axes. J-index refers to the fabric strength.

in the dunite and Troctolite A show a narrow range of composition ($Fo = 88.2\text{--}89.1$ mol %; Figs 10a and 14b; $Mg\# = 89\text{--}91$ mol %; Fig. 14c). These constant compositions of the mafic minerals (forsterite in olivine and Mg-number in clinopyroxene) are coupled with significant within-sample variations in plagioclase anorthite contents ($An = 52.9\text{--}66.8$ mol %; Fig. 14a and b), and therefore do not follow the compositional trends of fractional crystallization defined by the oceanic gabbroic sequences (South-West Indian Ridge, Dick *et al.*, 2002; Mid-Atlantic Ridge, Ross & Elthon, 1997; Lissenberg & Dick, 2008; Suhr *et al.*, 2008; Drouin *et al.*, 2009; Miller *et al.*, 2009). These peculiar compositional trends (Fig. 14a and b) are indicative of the buffering of the melt Mg-number by olivine-dissolving, reactive porous flow percolation (e.g. Collier & Kelemen, 2010; Sanfilippo *et al.*, 2016b; Borghini *et al.*, 2018). Mineral compositions in Troctolite A are similar to those documented in the amagmatic easternmost South-West Indian Ridge troctolites and olivine gabbros ($61\text{--}67^\circ E$; Paquet *et al.*, 2016). These peculiar mineral chemistry covariations were attributed to melt–rock interaction processes involving olivine and orthopyroxene dissolution by a percolating Na-rich basic melt, and subsequent crystallization of plagioclase and clinopyroxene.

Thermodynamic model of olivine-consuming reactive crystallization

To better constrain and quantify the role of reactive crystallization in the formation of the peculiar An–Fo and An–Mg# compositional trends in the Erro–Tobbio troctolitic body (Fig. 14a and b), we performed an assimilation–fractional crystallization (AFC) geochemical modelling calculation, assuming variable dissolved mass of olivine and concomitant melt crystallization, using the pMELTS thermodynamic program (Ghiorso *et al.*, 2002). This model aims at reproducing the diffuse reactive percolation of a high-temperature melt ($1270^\circ C$) into the shallow lithospheric mantle. Based on mineral–mineral partitioning, Rampone *et al.* (2016) documented a high temperature of equilibration ($>1100\text{--}1200^\circ C$) in both troctolites and host peridotites. The interaction process thus occurred at relatively high mantle temperatures.

The Erro–Tobbio ultramafic body does not include any basaltic intrusions, precluding direct information on the Troctolite A parental melt composition. However, a few unaltered primitive basaltic intrusions [loss on ignition (LOI) $< 2\%$; $Mg\# > 70$ mol %] have been documented in the Alpine–Apennine ophiolites. The initial melt composition adopted is a primitive MORB-type basalt ($Mg\# = 70.75$ mol %) associated with the Pineto gabbroic suite (Saccani *et al.*, 2008; Alpine ophiolite), the composition of which is given in Table 7. This primitive melt is characterized by a relatively low Ca/Na ratio ($Ca\# = 61.54$ mol %), most probably as the result of low degrees of mantle melting (Klein & Langmuir, 1987; Montanini *et al.*, 2008; Saccani *et al.*,

2008; Renna *et al.*, 2018), similar to what was described at the easternmost South-West Indian Ridge ($Ca\# = 55\text{--}60$ mol %; Paquet *et al.*, 2016). Such an Na-rich parental melt composition is consistent with the Alpine–Apennine compositional field of gabbroic rocks (Fig. 14c; Hébert *et al.*, 1989; Tribuzio *et al.*, 1999; Montanini *et al.*, 2008; Sanfilippo & Tribuzio, 2013), showing more Na-rich plagioclase compositions (at a given Mg-number in clinopyroxene) than the oceanic gabbroic series at the South-West Indian Ridge and Mid-Atlantic Ridge (Fig. 14c).

We modelled isobaric ($P = 4$ kbar) reactive fractional crystallization of the primitive MORB melt, cooling in steps of $5^\circ C$ while dissolving a fixed mass of olivine (0 g, 1 g, 2 g, 3 g per 100 g of melt) per $1^\circ C$ of cooling (Fig. 16). Similar models of reactive crystallization using the pMELTS thermodynamic program (Ghiorso *et al.*, 2002) have been previously performed by Collier & Kelemen (2010) and Sanfilippo *et al.* (2016), involving the assimilation of mantle lherzolite at 6 kbar. In the Erro–Tobbio, Troctolite A includes decimetre-size dunitic pods (Fig. 2d) preserved from melt impregnation, and no mantle pyroxene relict is found in any dunite or troctolite sample. This suggests that the protolith of the Erro–Tobbio troctolite was a dunite. Microstructures in Troctolite A indicate the late crystallization of poikilitic clinopyroxene in minor proportions (Table 1; Fig. 5b), therefore suggesting relatively low crystallization pressures (< 7 kbar), leading to the late saturation of clinopyroxene on a MORB-type melt liquid line of descent (Husen *et al.*, 2016). Based on field and microstructural observations, and previous geobarometric estimates within Troctolite A (3–5 kbar; Borghini *et al.*, 2007), we decided to model the dissolution of 100% olivine Fo_{89} (olivine composition in the dunite pods) at variable assimilation rates (see below) during a reactive fractional crystallization process occurring at 4 kbar. Recent experimental work (Borghini *et al.*, 2018; Francomme, 2018) demonstrated the possible replacive formation of an olivine-rich troctolite from a dunite protolith and the efficient buffer of the melt composition towards high Mg-numbers by olivine assimilation. They also demonstrated that the reactivity of a melt saturated in olivine (AH6; Husen *et al.*, 2016) with a dunitic matrix of Fo_{90} is driven by the chemical disequilibrium between the olivine forming the dunitic matrix (more forsteritic) and the olivine in equilibrium with the melt (see also Liang, 2003). The partial dissolution of the dunitic matrix is thus associated with the precipitation of an olivine of different composition that is in equilibrium with the modified melt.

Figure 16 shows the computed crystal line of descent of olivine, plagioclase and clinopyroxene, and Supplementary Data Table S6 reports the evolution of the melt and mineral compositions during fractional and reactive crystallization. The computed crystallization order is olivine–plagioclase–clinopyroxene, as expected from the crystallization of a MORB melt at low pressures (< 7 kbar; Bender *et al.*, 1978; Husen *et al.*,

Table 7: Input and output melt compositions of pMELTS numerical simulations of reactive and fractional crystallization

| wt % | SiO ₂ | TiO ₂ | Al ₂ O ₃ | Fe ₂ O ₃ | FeO | MnO | MgO | CaO | Na ₂ O | K ₂ O | Total | Mg# | Ca# | Liquidus temperature (°C) | ΔT_{liq} |
|--------------------------------|------------------|------------------|--------------------------------|--------------------------------|------|------|-------|-------|-------------------|------------------|-------|-------|-------|---------------------------|-------------------------|
| Initial melt* | 49.93 | 1.21 | 16.85 | 0.87 | 7.01 | 0.13 | 9.5 | 10.45 | 3.61 | 0.03 | 99.59 | 70.75 | 61.54 | 1261 | 0 |
| 5 g assimilation [†] | 49.5 | 1.16 | 16.05 | 0.85 | 7.11 | 0.13 | 11.4 | 9.95 | 3.44 | 0.03 | 99.62 | 74.08 | 61.51 | 1297 | 36 |
| 10 g assimilation [†] | 49.11 | 1.1 | 15.32 | 0.84 | 7.21 | 0.12 | 13.12 | 9.50 | 3.28 | 0.03 | 99.63 | 76.43 | 61.55 | 1322 | 61 |
| 15 g assimilation [†] | 48.75 | 1.05 | 14.65 | 0.83 | 7.3 | 0.12 | 14.7 | 9.09 | 3.14 | 0.03 | 99.66 | 78.21 | 61.53 | 1344 | 83 |
| Modified melt [‡] | 52.81 | 1.94 | 15.82 | 0.77 | 5.50 | 0.00 | 8.03 | 10.68 | 4.41 | 0.04 | 100.0 | 72.24 | 57.23 | 1222 | – |

Mg# = Mg/(Mg + Fe); Ca# = Ca/(Ca + Na); $-\Delta T_{\text{liq}} = T_{\text{liq}}(\text{modif}) - T_{\text{liq}}(\text{initial})$. Major elements in wt %.

*Initial primitive melt composition used for fractional and reactive crystallization modelling, after [Saccani et al. \(2008\)](#).

[†]Melt composition and liquidus temperature after assimilation of 5, 10 and 15 g of olivine during 5°C cooling.

[‡]Melt composition modified after reactive crystallization process, used as initial melt for fractional crystallization process of the olivine gabbros.

2016). The starting melt composition is in equilibrium with an olivine Fo = 87 mol %, but at increasing dissolution rates (from 0 to 3 g °C⁻¹ of cooling) the equilibrium forsterite content in olivine and the Mg-number in clinopyroxene are progressively buffered by the composition of the dissolved olivine (Fo = 89 mol %). It is worth noting that this extensive olivine dissolution implies the crystallization of new olivine crystals and/or recrystallization of the olivine matrix throughout the reactive percolation process ([Supplementary Data Table S6](#); [Liang, 2003](#)). [Supplementary Data Table S6](#) shows that even at high dissolution rates (3 g °C⁻¹ of cooling), the early stages of reactive crystallization (1270–1260°C), characterized by crystallization of olivine only, do not involve a significant variation in melt mass (olivine dissolved/olivine crystallized = 0.88–1.12). This supports the dissolution–reprecipitation of the pre-existing dunitic matrix. Moreover, given that in Troctolite A, most small undeformed olivine crystals embedded in poikilitic plagioclase and clinopyroxene are the result of extensive corrosion and disruption of large olivine grains (and therefore do not represent newly formed magmatic olivines; see Discussion), it is likely that olivine precipitation mostly consisted in the recrystallization of the pre-existing olivine rims ([Liang, 2003](#); [Morgan & Liang, 2005](#)). However, no compositional variation was found between the olivine cores (possibly relict) and rims (possibly recrystallized) ([Fig. 12i–l](#)). This is presumably due to the similar composition of the pre-existing (Fo = 89 mol %; [Table 2](#)) and recrystallized olivine (Fo ≈ 88 mol %; [Supplementary Data Table S6](#)), and to the fast Mg–Fe diffusion rates of olivine at magmatic temperatures ($t_{\text{equ}} < 200$ years for 3 mm radius; [Dohmen & Chakraborty, 2007](#); [Ferrando et al., 2018](#)).

During the reactive fractional crystallization process, the anorthite contents in plagioclase evolve freely towards lower values along the crystal line of descent ([Fig. 16](#)), leading to the reactive crystallization trends of variation previously described by [Collier & Kelemen \(2010\)](#) and [Sanfilippo et al. \(2016\)](#) (decreasing anorthite contents in plagioclase at constant forsterite contents in olivine and Mg-number in clinopyroxene). Crystal lines of descent at high rates of olivine dissolution during reactive crystallization (from 2 to 3 g °C⁻¹ of cooling) fit well the analyzed peculiar trends of mineral covariation

in the Erro–Tobbio troctolites and confirm the strong implication of olivine-dissolving reactive porous flow processes in the formation of the host Troctolite A from a pre-existing dunite ([Figs 15 and 16](#)).

Clinopyroxene cores from Troctolite A have high Cr₂O₃ contents ([Fig. 11a and c](#)), similar to those described in oceanic gabbroic rocks analyzed at the Mid-Atlantic Ridge ([Lissenberg & Dick, 2008](#); [Lissenberg & MacLeod, 2016](#); [Ferrando et al., 2018](#)), easternmost South-West Indian Ridge ([Paquet et al., 2016](#)) and Godzilla Megamullion ([Sanfilippo et al., 2016b](#)), and in olivine-rich troctolites from the Internal Liguride ophiolite ([Renna & Tribuzio, 2011](#); [Renna et al., 2016](#)). Although pMELTS ([Ghiorso et al., 2002](#)) does not allow the Cr₂O₃ compositional modelling of clinopyroxene, the process of partial dissolution and recrystallization of a dunite (olivine + spinel) described above could well explain the Cr₂O₃ enrichments observed in the clinopyroxene cores ([Fig. 11a and c](#)). Within Troctolite A, interstitial minerals often develop embayments on corroded relicts of spinel grains. This indicates partial dissolution of Cr-rich spinel (Cr# = 55–65 in the dunite; [Table 6](#)) together with the olivine during the reactive melt percolation process, as was previously described in oceanic settings and in the Internal Liguride ophiolites during replacive formation of olivine-rich gabbroic rocks ([Lissenberg & Dick, 2008](#); [Renna & Tribuzio, 2011](#); [Lissenberg & MacLeod, 2016](#); [Paquet et al., 2016](#); [Renna et al., 2016](#); [Sanfilippo et al., 2016b](#); [Ferrando et al., 2018](#)). The corrosion of spinel leads to Cr₂O₃ enrichments in the reacting melt, therefore explaining the Cr-rich compositions of clinopyroxenes crystallized from the percolating modified melt ([Fig. 11a](#)). The corrosion of spinel during impregnation of the dunite and the Cr-rich character of the melt are also suggested within Troctolite A by the crystallization of numerous fine-grained euhedral spinels associated with the poikilitic plagioclase ([Fig. 6d](#)).

Magmatic origin of Troctolite B

In Troctolite B, pseudo-tabular bodies crosscut the Troctolite A structures, with irregular to straight contacts with the host troctolite ([Figs 2c, 3a, b and 4](#)). Troctolite B has a lower modal content of olivine (from 45 to 60 vol. % modal olivine), with respect to the host

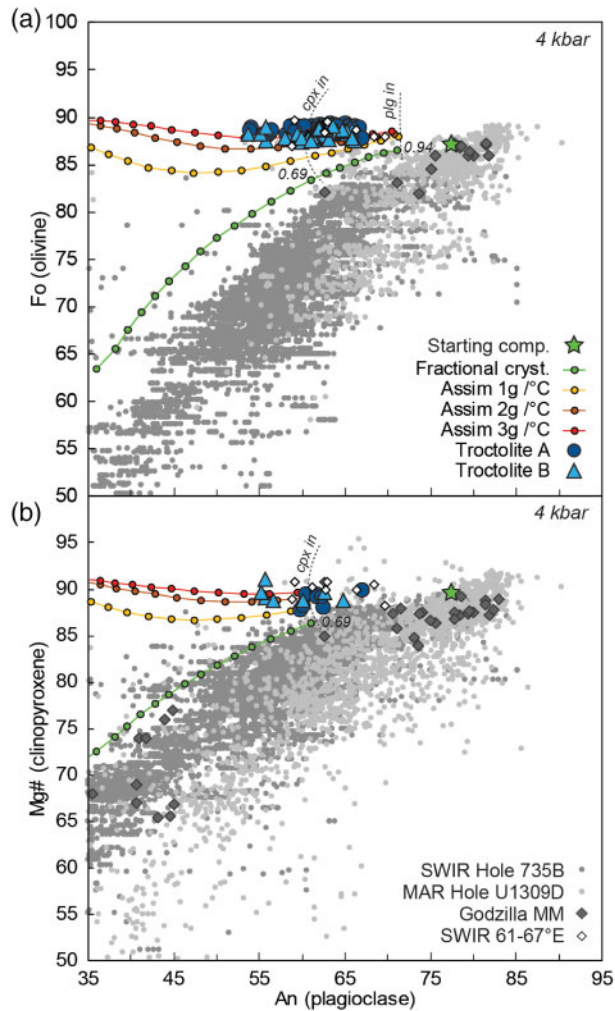


Fig. 16. pMELTS numerical simulations (Ghiorso *et al.*, 2002) of the major element compositions of plagioclase (anorthite content) vs (a) olivine (forsterite content), and (b) clinopyroxene (Mg-number) during fractional crystallization and reactive crystallization of a sodic primitive MORB, after Saccani *et al.* (2008) (see text for details). Varying assimilation rates of a dunite (100% olivine) from 1 to 3g °C⁻¹ of cooling are modelled, and compared with the core compositions of olivine–plagioclase, and clinopyroxene–plagioclase pairs analyzed in Troctolite A and Troctolite B. The green star represents the mineral compositions in equilibrium with the starting melt, and each dot along the crystal line of descent corresponds to a 5°C cooling step. The numbers along the fractional crystallization trend represent the remaining melt fraction at the saturation of plagioclase and clinopyroxene. Compositional fields for oceanic gabbroic suites are plotted for comparison: South-West Indian Ridge (SWIR Hole 735B: Dick *et al.*, 2002; SWIR 61–67°E: Paquet *et al.*, 2016); Mid-Atlantic Ridge (MAR; Ross & Elthon, 1997; Lissenberg & Dick, 2008; Suhr *et al.*, 2008; Drouin *et al.*, 2009; Miller *et al.*, 2009) and the Godzilla Megamullion (Godzilla MM; Harigane *et al.*, 2011; Sanfilippo *et al.*, 2013).

Troctolite A (from 55 to 97% modal olivine). The olivine matrix within Troctolite B shows extreme textural variations (Figs 3b–e and 6e), from millimetre-size euhedral (Fig. 7a) to centimetre-size hopper (Fig. 7b) to centimetre- to decimetre-size skeletal and dendritic crystals (Fig. 7c and d) (Rampone *et al.*, 2016). Hopper and

dendritic morphologies of olivine have been previously described in the Rum Layered Intrusion (Donaldson, 1974, 1977, 1982; O’Driscoll *et al.*, 2007), in olivine-rich troctolites from the Ligurian ophiolites (Renna *et al.*, 2016) and in crystallization experiments (Donaldson, 1976, 1977; Faure *et al.*, 2003, 2007) resulting from rapid disequilibrium crystallization of an undercooled melt (driven by a difference between the liquidus temperature of the melt and the melt temperature).

Olivine CPO in the granular portion of Troctolite B shows random orientations of the [100] axis, strong concentrations of the [010] axis normal to the foliation, and the [001] axis being the strongest axis concentration within the foliation plane (Fig. 9). In gabbroic intrusions, similar olivine CPOs are observed, correlated with strong orientations of the plagioclase [010] axis normal to the foliation plane (parallel to the [010] axis of olivine) (Fig. 9). Benn & Allard (1989) and Jousselein *et al.* (2012) previously described such CPOs of olivine in the Oman lower crustal layered gabbros and interpreted these orientations as the shape-related physical orientation of the crystals during magmatic flow.

Based on the crosscutting relationships between Troctolite B and the host Troctolite A (Figs 2b and 3a, c), the textural variability of olivine (Figs 3b–e and 6e), and the CPO indicative of magmatic flow within the granular part of Troctolite B (Fig. 9), we infer that Troctolite B originated as a magmatic segregation within hot, pre-existing Troctolite A during focused percolation of the melt modified after the diffuse reactive percolation forming Troctolite A (see the modelling below). The irregular contacts between the Troctolite B intrusions and the host Troctolite A indicate a brittle–ductile rheological behaviour, thus suggesting a minor temperature difference (<50°C) between the system and the intruding melt. The rheological evolution from diffuse percolation (forming Troctolite A) to focused percolation (related to a slight decrease in the temperature of the system) allowed higher quantities of melt to segregate and to form a magmatic flow (Fig. 9), leading to the crystallization of Troctolite B.

The mineral major element compositions of olivine, plagioclase and clinopyroxene in Troctolite B are less variable than in Troctolite A. The forsterite contents in olivine (Fo = 87.3–89.2; Figs 10a and 14b, c), the Mg-numbers (Mg# = 88.2–91; Figs 11 and 14a, c) and Cr₂O₃ contents in clinopyroxene (up to Cr₂O₃ = 1.55 wt %; Fig. 11a and c), and the anorthite contents in plagioclase (An = 55.1–66.1; Fig. 14) are in the same range of composition as previously described in Troctolite A. The geochemical model (using pMELTS; Ghiorso *et al.*, 2002) of reactive fractional crystallization developed for the host Troctolite A (Fig. 16) also fits the major element compositions of the Troctolite B mineral pairs, showing constant forsterite contents in olivine and Mg-numbers in clinopyroxene at decreasing anorthite contents in plagioclase (Figs 14b, c and 16). This indicates that the magmatic Troctolite B crystallized from the melt modified after the diffuse reactive percolation originating

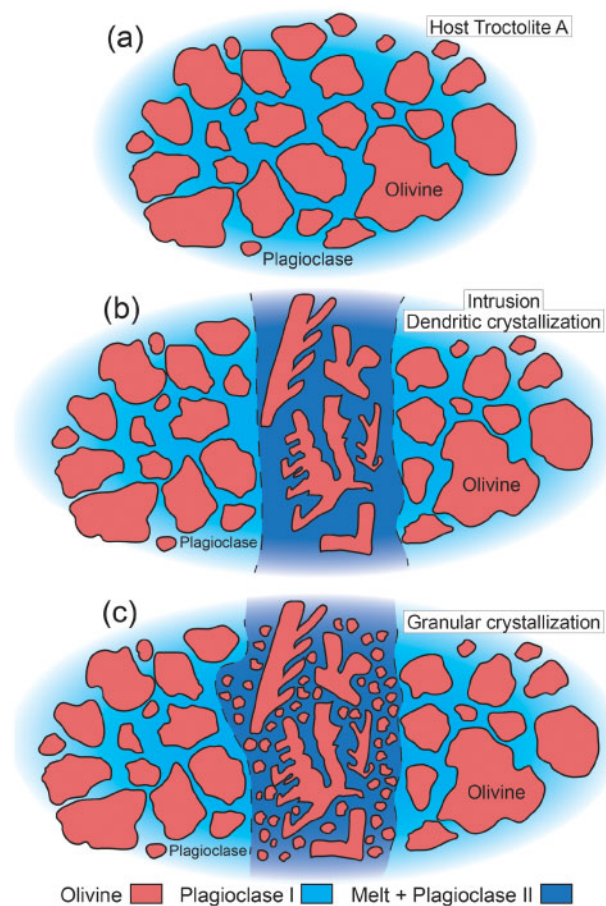


Fig. 17. Representative sketches for the formation of Troctolite B. (a) Initial state, host Troctolite A crystal mush. (b) Prior crystallization of dendritic olivine from the undercooled melt. (c) Equilibrium crystallization of fine-grained granular olivine.

Troctolite A. [Table 7](#) reports the initial melt composition and liquidus temperature of the Pineto primitive MORB melt used in the thermodynamic model of fractional and reactive crystallization (see Discussion), and the modified melt composition and liquidus temperature computed using pMELTS ([Ghiorso et al., 2002](#)), after dissolution of 5, 10 and 15 g of olivine (corresponding to a 5°C step of cooling for the modelled 1, 2 and 3 g °C⁻¹; [Fig. 16](#)). It should be noted that the modified compositions reported in [Table 7](#) consider only the dissolution of the olivine matrix during a 5°C cooling step, and not the subsequent precipitation of olivine from the melt. This approach allows us to compute the maximum increase in liquidus temperature driven by olivine assimilation ([Table 7](#)) in the modified melts, and therefore to assess the maximum degree of undercooling developed prior to olivine reprecipitation. The dissolution of olivine leads to a local increase of the Mg-number of the melt, resulting in an increase of the liquidus temperature of the melt of up to 83°C (relative to the liquidus temperature of the initial melt), for the assimilation of 15 g of olivine during one 5°C step of cooling (3 g °C⁻¹ of cooling; [Ghiorso et al., 2002](#); [Table 7](#)). Hence, the described process of partial dissolution of the

olivine matrix is able to rapidly develop a significant degree of undercooling of the melt, by increasing its liquidus temperature at almost constant melt temperature. We infer that the textural variability of olivine observed within the magmatic Troctolite B is the result of local changes in the degree of undercooling of the segregated melt, as was previously described for the Rum layered intrusion ([Donaldson, 1974, 1976, 1977, 1982](#); [O'Driscoll et al., 2007](#)). Crystallization experiments of mafic–ultramafic melts performed over a range of degrees of undercooling and cooling rates ([Donaldson et al., 1975](#); [Donaldson, 1976, 1977](#); [Faure et al., 2003, 2007](#)) have highlighted the possible development of hopper and dendritic olivine morphologies at degrees of undercooling as low as 10–20°C. Olivine dissolution involved in the reactive formation of Troctolite A is therefore a very good candidate to explain the skeletal and dendritic morphologies of magmatic olivine crystallized in Troctolite B.

The lack of significant geochemical variation between the different olivine morphologies (granular, hopper and skeletal) precludes the identification of a clear scenario for their formation sequence. However, slightly more evolved major element compositions of olivine (Fo = 87.5–88, [Fig. 10](#)), plagioclase (An = 60–62, [Fig. 13](#)) and clinopyroxene (Mg# = 88.7–89.5) in the granular part of Troctolite B (MF46A, [Table 1](#)) possibly imply later crystallization, after the rapid growth of skeletal dendritic olivines. Moreover, [O'Driscoll et al. \(2007\)](#) previously proposed for the Rum layered intrusion that the absence of initial suspended olivine in the primitive magmatic flow may favour the development of melt undercooling. These arguments point to a model of formation of Troctolite B in which dendritic olivines rapidly formed in the undercooled melt, prior to its evolution and the crystallization of the granular olivines ([Fig. 17](#)).

Intrusion of the modified melt—formation of the gabbroic intrusions

Gabbroic intrusions crosscut both the troctolitic body and the associated impregnated plagioclase lherzolites and have straight contacts with their host-rocks ([Borghini & Rampone, 2007](#); [Borghini et al., 2007](#); [Rampone et al., 2016](#)). Olivines and plagioclases from the gabbroic intrusions show CPO consistent with the shape-related orientation of the crystals in a magmatic flow ([Benn & Allard, 1989](#); [Jousselin et al., 2012](#)). Major element compositions of the rock-forming minerals (forsterite content of olivine, anorthite content of plagioclase and Mg-number in clinopyroxene) show a positive correlation and an evolution following a fractional crystallization trend, parallel to the compositional trends reported for oceanic gabbroic series at the Mid-Atlantic Ridge ([Fig. 14b and c](#)) ([Ross & Elthon, 1997](#); [Lissenberg & Dick, 2008](#); [Suhr et al., 2008](#); [Drouin et al., 2009](#); [Miller et al., 2009](#); [Ferrando et al., 2018](#)) and the South-West Indian Ridge ([Dick et al., 2002](#)). However, although showing similar mineral geochemical trends of

evolution to the oceanic gabbroic series, their compositions are shifted towards higher forsterite contents in olivine and Mg-numbers in clinopyroxene at a given anorthite content in plagioclase (Fig. 14b and c). The most primitive gabbroic intrusions show mineral major element compositions similar to those in Troctolite B, thus indicating a common parental melt. Accordingly, we infer that the gabbroic intrusions formed by fractional crystallization of the melt modified after the reactive fractional crystallization that formed Troctolites A and B (Fig. 16), at lower temperatures allowing for brittle behaviour and emplacement of the melt in fractures (Borghini *et al.*, 2007; Rampone & Borghini, 2008).

To test this hypothesis, we performed a geochemical modelling study of fractional crystallization (using pMELTS; Ghiorso *et al.*, 2002) using as a starting melt the output modified melt composition after previous reactive fractional crystallization (Fig. 18; Table 7). As shown in Fig. 18, the fractional crystallization of the modified melt reproduces the chemical covariation arrays observed in the gabbroic intrusions, almost parallel to the trends defined by oceanic gabbroic suites, but shifted towards more Mg-rich mineral compositions of olivine (forsterite content) and clinopyroxene (Mg-number). This confirms that the parental melt of the gabbroic intrusions corresponds to the melt modified after formation of Troctolites A and B, and that no further melt–rock interaction was involved in the fractional crystallization process.

Constraints on the geodynamic context and melt–rock interaction processes

Geochronological data for the Erro–Tobbio gabbroic intrusions (Sm–Nd, 178 ± 5 Ma; Rampone *et al.*, 2014), together with gabbroic rocks from the External Liguride units (170–179 Ma Northern Apennines; Tribuzio *et al.*, 2004), yield the oldest ages available for the gabbroic crust of the Ligurian Tethys ocean. These ages are older than the age of continental break-up and onset of oceanization of the Ligurian Tethys (164–166 Ma; Manatschal & Müntener, 2009). Also, they indicate an ~ 10 Myr time gap between the early emplacement of the Erro–Tobbio and External Liguride gabbros, and the main magmatic activity of the Ligurian Tethys (155–165 Ma; Rampone *et al.*, 2014, and references therein). Accordingly, the Erro–Tobbio gabbroic intrusions have been interpreted as evidence of early magmatism in thinned lithospheric mantle exhumed in an ocean–continent transition setting during the onset of Jurassic lithospheric extension (Fig. 19a; Manatschal & Müntener, 2009; Rampone *et al.*, 2014). The scarcity of gabbroic and basaltic bodies in the Alpine–Apennine ophiolites (e.g. Marroni *et al.*, 1998; Tribuzio *et al.*, 2000, 2004; Montanini *et al.*, 2008; Saccani *et al.*, 2008), and the Na-rich composition of the basaltic parental melts (Fig. 14c; Saccani *et al.*, 2008; see Discussion) are consistent with low-degree melting of the upwelling mantle in a slow- to ultraslow-spreading environment (Klein &

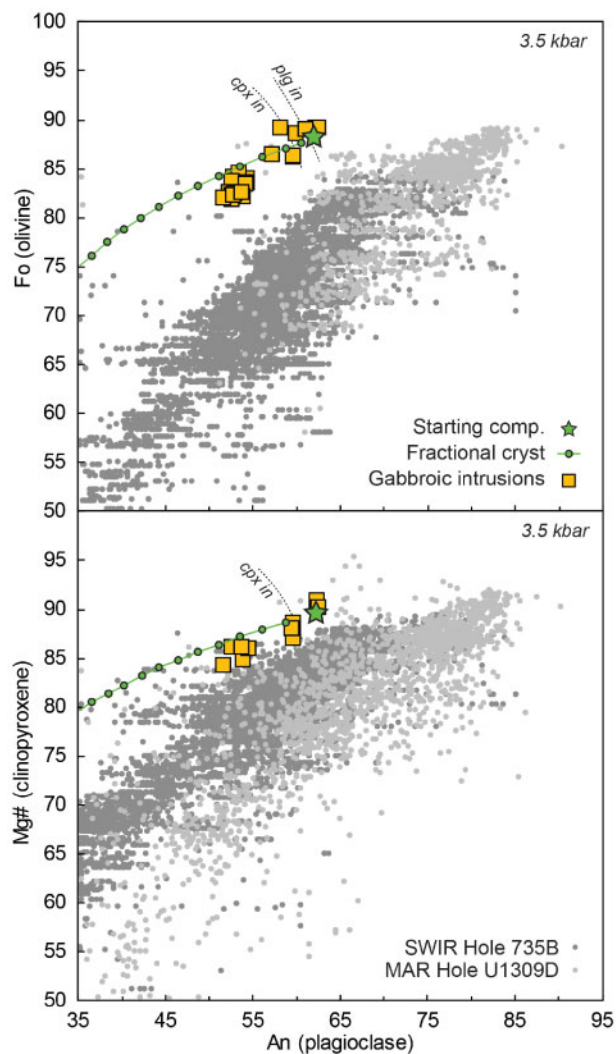


Fig. 18. pMELTS numerical modelling (Ghiorso *et al.*, 2002) of the major element compositions of olivine (forsterite content), plagioclase (anorthite content) and clinopyroxene (Mg-number) during fractional crystallization of the melt modified after reactive equilibrium crystallization and formation of Troctolite A and Troctolite B, compared with the major element core compositions of olivine–plagioclase and clinopyroxene–plagioclase pairs analyzed from the Erro–Tobbio gabbroic intrusions. The green star represents the mineral compositions in equilibrium with the starting melt, and each dot along the crystal line of descent corresponds to a 5°C cooling step. Compositional fields of oceanic gabbroic suites are as in Fig. 16.

Langmuir, 1987; Montanini *et al.*, 2008; Saccani *et al.*, 2008; Renna *et al.*, 2018; Fig. 19a).

Our structural data, showing the partial preservation of the protolith axial [100] olivine CPO during replacive formation of Troctolite A (Fig. 8), point to a percolation process occurring at variable instantaneous melt/rock ratios, in an overall low melt supply regime (Fig. 15; see Discussion). Also, our thermodynamic models show that extensive dissolution–precipitation reactions are needed during the multi-stage formation of Troctolite A and Troctolite B to explain their peculiar compositional trends (Figs 16 and 19b; see Discussion). As demonstrated by several mass-balance and AFC models

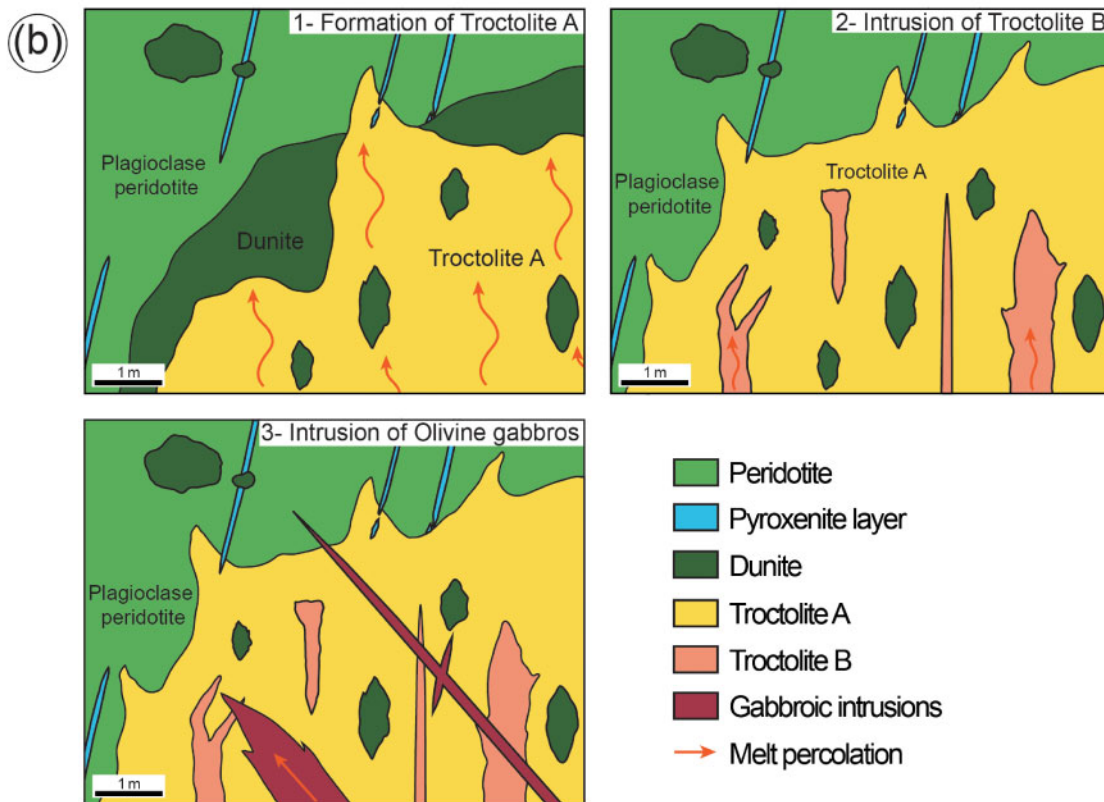
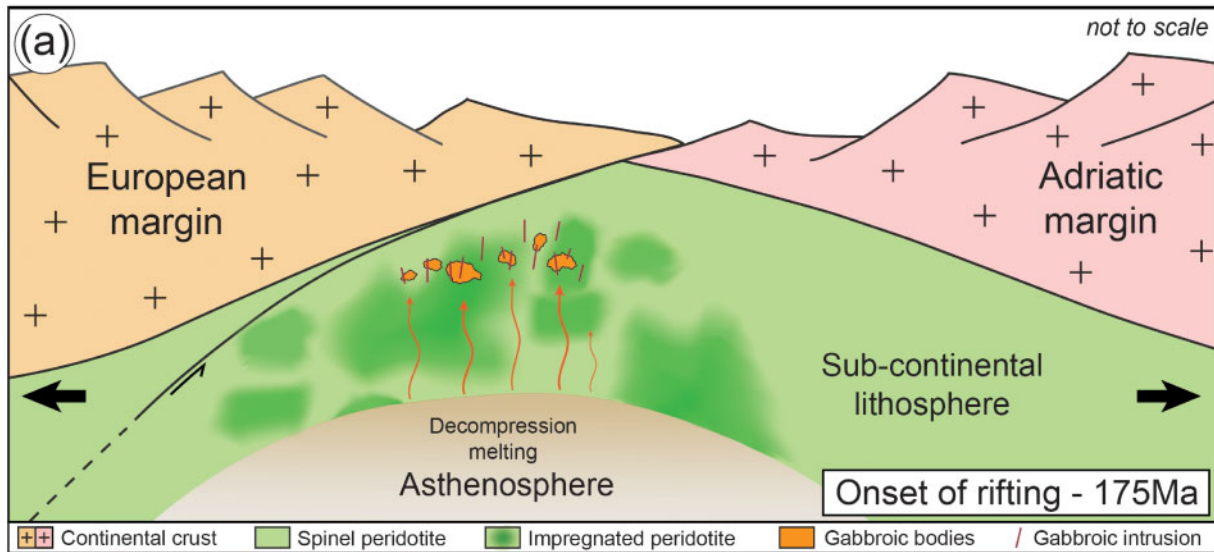


Fig. 19. Interpretative sketches of the geological context and evolution of the peridotitic and troctolitic body. (a) Geological context of the formation of the Erro-Tobbio troctolitic body at 175 Ma, during the onset of the Ligurian Tethys basin rifting. (b) Representative replacive formation of Troctolite A from a dunitic protolith, intrusion of Troctolite B during focused melt percolation and intrusion of gabbroic rocks in fractures.

(Lissenberg & Dick, 2008; Sanfilippo *et al.*, 2015b; Paquet *et al.*, 2016; Rampone *et al.*, 2016), modifications of the melt composition during melt-rock interaction are possible only at low melt supply conditions. Core-rim composition profiles in interstitial phases from Troctolite A (plagioclase and clinopyroxene, Fig. 12a-h) show decreasing Cr_2O_3 and Al_2O_3 , and increasing TiO_2 concentrations in clinopyroxene towards the rim

(<200 μm from the contact with olivine), and decreasing anorthite content and CaO and Al_2O_3 concentrations towards the plagioclase rim. These core-rim chemical zonation in interstitial clinopyroxene and plagioclase suggest an *in situ* evolution of the melt composition during reactive crystallization at decreasing melt mass (Borghini & Rampone, 2007; Borghini *et al.*, 2007; Rampone & Borghini, 2008). This indicates that the

process forming the replacive Troctolite A is not characterized by constant replenishment and efficient extraction of the melt (Fig. 19b), but rather by sparse melt injections, the chemical compositions of which were dominated by the dissolution–precipitation processes.

Mineral reactive compositional trends (constant Mg# of olivine and clinopyroxene at variable An content in plagioclase), similar to those observed in the Erro–Tobbio troctolitic body, have been documented in olivine-rich troctolites from slow-spreading oceanic environments at the easternmost South-West Indian Ridge (Fig. 16; Paquet *et al.*, 2016) and at the Godzilla Megamullion (Fig. 16; Sanfilippo *et al.*, 2016b). Both these settings are characterized by scarce basaltic and gabbroic intrusions in kilometres of exhumed mantle peridotites. In these troctolites, peculiar compositional trends in minerals have been interpreted as the result of extensive melt–rock interaction processes involving low magma supplies and melt/rock ratios (Paquet *et al.*, 2016; Sanfilippo *et al.*, 2016b).

Replacive olivine-rich troctolites have also been described from the Atlantis Massif [Integrated Ocean Drilling Program (IODP) Hole U1309D; Blackman *et al.*, 2006; Suhr *et al.*, 2008; Drouin *et al.*, 2009, 2010; Ferrando *et al.*, 2018], associated with a 1415 m long crustal section (>90% gabbroic rocks; Blackman *et al.*, 2006). Interestingly, the mineral compositions of these olivine-rich troctolites and associated gabbroic crust follow a trend of fractional crystallization at ~2 kbar (Miller *et al.*, 2009). This indicates that the global composition of the percolating MORB melt was not modified during the melt–rock interaction processes and formation of replacive olivine-rich troctolites (Ferrando *et al.*, 2018). Consistently, structural data for the olivine CPO within the olivine-rich troctolites from the Atlantis Massif suggest high melt supply and melt/rock ratios involved in the melt percolation and dissolution–precipitation reactions (Drouin *et al.*, 2010; Ferrando *et al.*, 2018). This further confirms that low melt/rock ratios are necessary to drive a significant modification of the melt composition during melt–rock interaction processes.

The context of formation of the Erro–Tobbio troctolitic body and associated gabbroic intrusions is therefore representative of a slow- to ultraslow-spreading system characterized by very low melt supply, therefore allowing the percolating melt composition to be controlled and buffered by the melt–rock interaction processes.

SUMMARY AND CONCLUSIONS

In the studied area, the Erro–Tobbio peridotites, troctolites and gabbroic intrusions record a multi-stage structural and geochemical evolution involving extensive dissolution–precipitation reactions. This can be summarized as follows.

(1) The formation of the replacive Troctolite A is related to diffuse reactive melt percolation in a pre-existing dunitic matrix (Fig. 19b). Mineral compositions

in Troctolite A and thermodynamic models indicate a melt–rock interaction-dominated process (Fig. 16), which involves olivine dissolution and crystallization of plagioclase and minor clinopyroxene.

(2) Subsequently, the focusing of melts modified after reactive percolation leads to the formation of pseudo-tabular Troctolite B magmatic bodies (Fig. 19b). High degrees of undercooling in the modified melt resulted in hopper to dendritic olivine morphologies during crystallization of Troctolite B (Fig. 17).

(3) The late gabbroic dykes, crosscutting the association between the impregnated plagioclase peridotites and Troctolites A and B, represent the product of fractional crystallization of the same modified melts (Fig. 19b).

The evolution from diffuse reactive percolation to focused reactive percolation, followed by intrusion and fractional crystallization of the gabbroic intrusions, is driven by the decreasing temperature of the exhuming system (Fig. 19a), controlling the rheology of the host-rock and the ability of the melt to segregate into magmatic intrusions. The geochemical similarities observed between Troctolite B and the most primitive gabbroic intrusions indicate a common modified parental melt, which allows us to link the focused percolation and intrusion events. Thus, the multi-stage formation of the troctolitic body and associated gabbroic intrusions (Fig. 19b) are related to a single thermal evolution of the ultramafic body, during the onset of opening of the Ligurian Tethys (Fig. 19a).

This study provides field-controlled constraints on the structural and geochemical modifications induced by melt–rock interaction processes, as a function of the involved melt/rock ratio. At low melt supply and melt/rock ratios, the structure of the protolith is preserved during reactive crystallization, and the melt composition can be easily controlled by the continuing dissolution–precipitation reactions. This leads to the observed buffering of the melt composition towards high Mg-numbers in the troctolitic body. In contrast, melt percolation involving high melt supply and melt/rock ratios leads to the loss of cohesion of the solid matrix and pre-existing structure. In such circumstances, the global melt composition cannot be modified during melt–rock interactions and the crystallized minerals follow a fractional crystallization trend, as documented at the Atlantis Massif.

ACKNOWLEDGEMENTS

We would like to thank Professor Joerg Hermann, Dr Alessio Sanfilippo and an anonymous reviewer for their constructive comments, which have improved the quality of the paper. We also thank Paolo Campanella and Alessandra Gavoglio, Christophe Nevado and Doriane Delmas for realization of the thin section and high-quality polishing, as well as Fabrice Barou for assistance with the EBSD analyses, Andrea Risplendente for assistance with the EPMA, Marco Scarsi and Nicola

Campomenosi for assistance with fieldwork, and Giulio Borghini for stimulating discussions.

FUNDING

This project has been supported by the People Programme (Marie Curie Actions) of the European Union's Seventh Framework Programme FP7/2007–2013/ under REA-Grant Agreement No. 608001, 'ABYSS', and by the Italian Ministry of Education, University and Research (MIUR) [PRIN-2015C5LN35] 'Melt–rock reaction and melt migration in the MORB mantle through combined natural and experimental studies'.

SUPPLEMENTARY DATA

Supplementary data are available at *Journal of Petrology* online.

REFERENCES

- Basch, V. (2018). Melt–rock interactions in the oceanic lithosphere: microstructural and petro-geochemical constraints from ophiolites. PhD thesis, Università degli Studi di Genova.
- Basch, V., Rampone, E., Crispini, L., Ferrando, C., Ildefonse, B. & Godard, M. (2018). From mantle peridotites to hybrid troctolites: textural and chemical evolution during melt–rock interaction history (Mt. Maggiore, Corsica, France). *Lithos* **323**, 4–23.
- Bender, J. F., Hodges, F. N. & Bence, A. E. (1978). Petrogenesis of basalts from the project FAMOUS area: experimental study from 0 to 15 kbars. *Earth and Planetary Science Letters* **41**, 277–302.
- Ben Ismail, W. & Mainprice, D. (1998). An olivine fabric database: an overview of upper mantle fabrics and seismic anisotropy. *Tectonophysics* **296**, 145–157.
- Benn, K. & Allard, B. (1989). Preferred mineral orientations related to magmatic flow in ophiolite layered gabbros. *Journal of Petrology* **30**, 925–946.
- Bezzi, A. & Piccardo, G. B. (1971). Structural features of the Ligurian ophiolites: petrologic evidence for the 'oceanic' floor of the Northern Apennines geosyncline: a contribution to the problem of the alpine-type gabbro–peridotite associations. *Memorie della Società Geologica Italiana* **10**, 53–63.
- Blackman, D. K., Ildefonse, B., John, B. E., Ohara, Y., Miller, D. J., MacLeod, C. J. & Expedition 304/305 Scientists (2006). Expedition 304/305 summary. In: Blackman, D. K., Ildefonse, B., John, B. E., Ohara, Y., Miller, D. J., MacLeod, C. J. & the Expedition 304/305 Scientists (eds) *Proceedings of the Integrated Ocean Drilling Program*, Vol. **304/305**. College Station, TX: Integrated Ocean Drilling Program, p. 60.
- Borghini, G. & Rampone, E. (2007). Postcumulus processes in oceanic-type olivine-rich cumulates: the role of trapped melt crystallization versus melt–rock interaction. *Contributions to Mineralogy and Petrology* **154**, 619–633.
- Borghini, G., Rampone, E., Crispini, L., De Ferrari, R. & Godard, M. (2007). Origin and emplacement of ultramafic–mafic intrusions in the Erro–Tobbio mantle peridotite (Ligurian Alps, Italy). *Lithos* **94**, 210–229.
- Borghini, G., Francomme, J. E. & Fumagalli, P. (2018). Melt–dunite interactions at 0.5 and 0.7 GPa: experimental constraints on the origin of olivine-rich troctolites. *Lithos* **323**, 44–57.
- Borsi, L., Schärer, U., Gaggero, L. & Crispini, L. (1996). Age, origin and geodynamic significance of plagiogranites in Iherzolites and gabbros of the Piedmont–Ligurian ocean basin. *Earth and Planetary Science Letters* **140**, 227–241.
- Boudier, F. & Nicolas, A. (1995). Nature of the transition zone in the Oman ophiolite. *Journal of Petrology* **36**, 777–796.
- Bunge, H. J. (1982). *Texture Analysis in Material Sciences*. London: Butterworths.
- Capponi, G., Crispini, L., Silvestri, R. & Vigo, E. (1999). The role of Early Miocene thrust tectonics in the structural arrangement of the Voltri Group (Ligurian Alps, Italy): evidence of Bandita area. *Ofioliti* **24**, 13–19.
- Ceuleneer, G. & Rabinowicz, M. (1992). Mantle flow and melt migration beneath oceanic ridges: models derived from observation in ophiolites, in mantle flow and melt generation at mid-ocean ridges. In: Morgan, J. P., Blackman, D. B. and Sinton, J. M. (eds) *Mantle Flow and Melt Generation at Mid-Ocean Ridges*. American Geophysical Union, *Geophysical Monograph Series*, **71**, 123–154.
- Chiesa, S., Cortesogno, L., Forcella, F., Galli, M., Messiga, B., Pasquarè, G., Pedemonte, G. M., Piccardo, G. B. & Rossi, P. M. (1975). Assetto strutturale ed interpretazione geodinamica del Gruppo di Voltri. *Bollettino della Società Geologica Italiana* **94**, 555–581.
- Collier, M. L. & Kelemen, P. B. (2010). The case for reactive crystallization at mid-ocean ridges. *Journal of Petrology* **51**, 1913–1940.
- Coumans, J. P., Stix, J., Clague, D. A., Minarik, W. G. & Layne, G. D. (2016). Melt–rock interaction near the Moho: evidence from crystal cargo in lavas from near-ridge seamounts. *Geochimica et Cosmochimica Acta* **191**, 139–164.
- Dick, H. J. B., Ozawa, K., Meyer, P. S., Niu, Y., Robinson, P. T., Constantin, M., Hebert, R., Maeda, J., Natland, J. H., Hirth, J. G. & Mackie, S. M. (2002). Primary silicate mineral chemistry of a 1.5-km section of very slow spreading lower ocean crust: ODP hole 735B, southwest Indian ridge. In: Natland, J. H., Dick, H. J. B., Miller, D. J. and Von Herzen, R. P. (eds) *Proceedings of the Ocean Drilling Program, Scientific Results, Vol. 176*. College Station, TX: Ocean Drilling Program, pp. 1–61.
- Dick, H. J. B., Tivey, M. A. & Tucholke, B. E. (2008). Plutonic foundation of a slow-spreading ridge segment: oceanic core complex at Kane Megamullion, 23°30'N, 45°20'W. *Geochemistry, Geophysics, Geosystems* **9**, Q05014.
- Dick, H. J. B., Lissenberg, C. J. & Warren, J. M. (2010). Mantle melting, melt transport, and delivery beneath a slow-spreading ridge: the paleo-MAR from 23°15'N to 23°45'N. *Journal of Petrology* **51**, 425–467.
- Dijkstra, A. H., Drury, M. R. & Frijihoff, R. M. (2002). Microstructures and lattice fabrics in the Hilti mantle section (Oman Ophiolite): evidence for shear localization and melt weakening in the crust–mantle transition zone? *Journal of Geophysical Research* **107**, 2270.
- Dijkstra, A. H., Barth, M. G., Drury, M. R., Mason, P. R. D. & Vissers, R. L. M. (2003). Diffuse porous melt flow and melt–rock reaction in the mantle lithosphere at a slow-spreading ridge: a structural petrology and LA-ICP-MS study of the Othris Peridotite Massif (Greece). *Geochemistry, Geophysics, Geosystems* **4**, 8613.
- Dohmen, R. & Chakraborty, S. (2007). Fe–Mg diffusion in olivine II: point defect chemistry, change of diffusion mechanisms and a model for calculation of diffusion coefficients in natural olivine. *Physics and Chemistry of Minerals* **34**, 409–430.
- Donaldson, C. H. (1974). Olivine crystal types in harristic rocks of the Rhum pluton and in Archean spinifex rocks. *Geological Society of American Bulletin* **85**, 1721–1726.

- Donaldson, C. H. (1976). An experimental investigation of olivine morphology. *Contributions to Mineralogy and Petrology* **57**, 187–213.
- Donaldson, C. H. (1977). Laboratory duplication of comb layering in the Rhum pluton. *Mineralogical Magazine* **41**, 323–336.
- Donaldson, C. H. (1982). Origin of some of the Rhum harrisite by segregation of intercumulus liquid. *Mineralogical Magazine* **45**, 201–209.
- Donaldson, C. H., Williams, R. J. & Lofgren, G. E. (1975). A sample holding technique for study of crystal growth in silicate melts. *American Mineralogist* **60**, 324–326.
- Drouin, M., Godard, M., Ildefonse, B., Bruguier, O. & Garrido, C. (2009). Geochemical and petrographic evidence for magmatic impregnation in the oceanic lithosphere at Atlantis Massif, Mid-Atlantic Ridge (IODP Hole U1309D, 30°N). *Chemical Geology* **264**, 71–88.
- Drouin, M., Ildefonse, B. & Godard, M. (2010). A microstructural imprint of melt impregnation in slow spreading lithosphere: olivine-rich troctolites from the Atlantis Massif, Mid-Atlantic Ridge, 30°N, IODP Hole U1309D. *Geochemistry, Geophysics, Geosystems* **11**, Q06003.
- Dygert, N., Liang, Y. & Kelemen, P. B. (2016). Formation of plagioclase lherzolite and associated dunite–harzburgite–lherzolite sequences by multiple episodes of melt percolation and melt rock reaction: an example from the Trinity ophiolite, California, USA. *Journal of Petrology* **57**, 815–838.
- Ernst, W. G. & Piccardo, G. B. (1979). Petrogenesis of some Ligurian peridotites: I. Mineral and bulk rock chemistry. *Geochimica et Cosmochimica Acta* **43**, 219–237.
- Faure, F., Trolliard, G., Nicollet, C. & Montel, J. M. (2003). A developmental model of olivine morphology as a function of the cooling rate and the degree of undercooling. *Contributions to Mineralogy and Petrology* **145**, 251–263.
- Faure, F., Schiano, P., Trolliard, G., Nicollet, C. & Soulestin, B. (2007). Textural evolution of polyhedral olivine experiencing rapid cooling rates. *Contributions to Mineralogy and Petrology* **153**, 405–416.
- Ferrando, C., Godard, M., Ildefonse, B. & Rampone, E. (2018). Melt transport and mantle assimilation at Atlantis Massif (IODP Site U1309): constraints from geochemical modelling. *Lithos* **323**, 24–43.
- Francomme, J. E. (2018). Melt–rock interaction at the mantle–crust transition zone in the oceanic spreading lithosphere: an experimental study. PhD thesis, Università degli Studi di Milano.
- Garrido, C. J. & Bodinier, J.-L. (1999). Diversity of mafic rocks in the Ronda peridotite: evidence for pervasive melt–rock reaction during heating of subcontinental lithosphere by upwelling asthenosphere. *Journal of Petrology* **40**, 729–754.
- Ghiorso, M. S., Hirschmann, M., Reiners, P. W. & Kress, V. C. I. (2002). The pMELTS: a revision of MELTS aimed at improving calculation of phase relations and major element partitioning involved in partial melting of the mantle at pressures up to 3 GPa. *Geochemistry, Geophysics, Geosystems*, **3**, 36.
- Godard, M., Bodinier, J.-L. & Vasseur, G. (1995). Effects of mineralogical reactions on trace element redistributions in mantle rocks during percolation processes: a chromatographic approach. *Earth and Planetary Science Letters* **133**, 449–461.
- Harigane, Y., Michibayashi, K. & Ohara, Y. (2011). Deformation and hydrothermal metamorphism of gabbroic rocks within the Godzilla Megamullion, Parece Vela Basin, Philippine Sea. *Lithos* **124**, 185–199.
- Hébert, R., Serri, G. & Hekinian, R. (1989). Mineral chemistry of ultramafic tectonites and ultramafic to gabbroic cumulates from the major oceanic basins and Northern Apennines ophiolites (Italy)—a comparison. *Chemical Geology* **77**, 183–207.
- Higgie, K. & Tommasi, A. (2012). Feedbacks between deformation and melt distribution in the crust–mantle transition zone of the Oman ophiolite. *Earth and Planetary Science Letters* **359–360**, 61–72.
- Higgie, K. & Tommasi, A. (2014). Deformation in a partially molten mantle: constraints from plagioclase lherzolites from Lanzo, western Alps. *Tectonophysics* **615–616**, 167–181.
- Hoogerduijn-Strating, E. H., Piccardo, G. B., Rampone, E., Scambelluri, M. & Vissers, R. L. (1990). The structure and petrology of the Erro–Tobbio peridotite, Voltri massif, Ligurian Alps: guidebook for a two-day-excursion with emphasis on processes in the upper mantle. *Ofioliti* **15**, 119–184.
- Hoogerduijn-Strating, E. H., Rampone, E., Piccardo, G. B., Drury, M. R. & Vissers, R. L. M. (1993). Subsolidus emplacement of mantle peridotites during incipient oceanic rifting and opening of the Mesozoic Tethys (Voltri Massif, NW Italy). *Journal of Petrology* **34**, 901–927.
- Husen, A., Renat, R. A. & Holtz, F. (2016). The effect of H₂O and pressure on multiple saturation and liquid lines of descent in basalt from the Shatsky Rise. *Journal of Petrology* **57**, 309–344.
- Jousselin, D., Nicolas, A. & Boudier, F. (1998). Detailed mapping of a mantle diapir below a paleo-spreading center in the Oman ophiolite. *Journal of Geophysical Research: Solid Earth* **103**, 18153–18170.
- Jousselin, D., Morales, L. F. G., Nicolle, M. & Stephant, A. (2012). Gabbro layering induced by simple shear in the Oman ophiolite Moho transition zone. *Earth and Planetary Science Letters* **331–332**, 55–66.
- Karato, S.-I., Jung, H., Katayama, I. & Skemer, P. (2008). Geodynamic significance of seismic anisotropy of the upper mantle: new insights from laboratory studies. *Annual Review of Earth and Planetary Sciences* **36**, 59–93.
- Kelemen, P. B., Hitehead, J. A., Aharonov, E. & Jordahl, K. A. (1995a). Experiments on flow focusing in soluble porous media, with applications to melt extraction from the mantle. *Journal of Geophysical Research: Solid Earth* **100**, 475–496.
- Kelemen, P. B., Shimizu, N. & Salters, V. J. M. (1995b). Extraction of mid-ocean-ridge basalt from the upwelling mantle by focused flow of melt in dunite channels. *Nature* **375**, 747–753.
- Kelemen, P. B., Braun, M. & Hirth, G. (2000). Spatial distribution of melt conduits in the mantle beneath oceanic spreading ridges: observations from the Ingalls and Oman ophiolites. *Geochemistry, Geophysics, Geosystems* **1**, 1999GC000012.
- Kelemen, P. B., Kikawa, E., Miller, D. J. & Shipboard Scientific Party (2007). Leg 209 summary: processes in a 20-km thick conductive boundary layer beneath the Mid-Atlantic Ridge, 14°–16°N. In: Kelemen, P. B., Kikawa, E. and Miller, D. J. (eds) *Proceedings of the Ocean Drilling Project, Scientific Results*, Vol. **209**. College Station, TX: Ocean Drilling Program, pp. 1–33.
- Klein, E. M. & Langmuir, C. H. (1987). Global correlations of ocean ridge basalt chemistry with axial depth and crustal thickness. *Journal of Geophysical Research* **92**, 8089–8115.
- Lambart, S., Laporte, D. & Schiano, P. (2009). An experimental study of focused magma transport and basalt–peridotite interactions beneath mid-ocean ridges: implications for the generation of primitive MORB compositions. *Contributions to Mineralogy and Petrology* **157**, 429–451.
- Laubier, M., Grove, T. L. & Langmuir, C. H. (2014). Trace element mineral/melt partitioning for basaltic and basaltic andesitic melts: an experimental and laser ICP-MS study with

- application to the oxidation state of mantle source regions. *Earth and Planetary Science Letters* **392**, 265–278.
- Le Roux, V., Tommasi, A. & Vauchez, A. (2008). Feedback between melt percolation and deformation in an exhumed lithosphere–asthenosphere boundary. *Earth and Planetary Science Letters* **274**, 401–413.
- Liang, Y. (2003). Kinetics of crystal–melt reaction in partially molten silicates: 1. Grain scale processes. *Geochemistry, Geophysics, Geosystems* **4**, doi:10.1029/2002GC000375.
- Liang, Y., Schiemenz, A., Hesse, M. A. & Parmentier, E. M. (2011). Waves, channels, and the preservation of chemical heterogeneities during melt migration in the mantle. *Geophysical Research Letters* **38**, L20308.
- Lissenberg, C. J. & Dick, H. J. B. (2008). Melt–rock reaction in the lower oceanic crust and its implications for the genesis of mid-ocean ridge basalt. *Earth and Planetary Science Letters* **271**, 311–325.
- Lissenberg, C. J. & MacLeod, C. J. (2016). A reactive porous flow control on mid-ocean ridge magmatic evolution. *Journal of Petrology* **57**, 2195–2220.
- Lissenberg, C. J., MacLeod, C. J., Howard, K. A. & Godard, M. (2013). Pervasive reactive melt migration through fast-spreading lower oceanic crust (Hess Deep, equatorial Pacific Ocean). *Earth and Planetary Science Letters* **361**, 436–447.
- Mainprice, D., Bachmann, F., Hielscher, R. & Schaebein, H. (2014). Descriptive tools for the analysis of texture projects with large datasets using MTEX: strength, symmetry and components. *Geological Society of London, Special Publications* **409**.
- Manatschal, G. & Müntener, O. (2009). A type sequence across an ancient magma-poor ocean–continent transition: the example of the western Alpine Tethys ophiolites. *Tectonophysics* **73**, 4–19.
- Marroni, M., Molli, G., Montanini, A. & Tribuzio, R. (1998). The association of continental crust rocks with ophiolites in the Northern Apennines (Italy): implications for the continent–ocean transition in the Western Tethys. *Tectonophysics* **292**, 43–66.
- Miller, D. J., Abratis, M., Christie, D., Drouin, M., Godard, M., Ildefonse, B., Maeda, J., Weinstein, A., Yamasaki, T., Suzuki, Y., Niino, A., Sato, Y. & Takeda, F. (2009). Data report: microprobe analyses of primary mineral phases from site U1309, Atlantis Massif, IODP Expedition 304/305. In: Blackman, D. K., Ildefonse, B., John, B. E., Ohara, Y., Miller, D. J., MacLeod, C. J. & the Expedition 304/305 Scientists (eds) *Proceedings of the International Ocean Drilling Program*, Vol. **304/305**. College Station, TX: Integrated Ocean Drilling Program, p. 4.
- Montanini, A., Tribuzio, R. & Vernia, L. (2008). Petrogenesis of basalts and gabbros from an ancient continent–ocean transition (External Ligurides ophiolites, Northern Italy). *Lithos* **101**, 453–479.
- Morgan, Z. & Liang, Y. (2005). An experimental study of the kinetics of lherzolite reactive dissolution with applications to melt channel formation. *Contributions to Mineralogy and Petrology* **150**, 369–385.
- Müntener, O., Pettke, T., Desmurs, L., Meier, M. & Schaltegger, R. (2004). Refertilization of mantle peridotite in embryonic ocean basins: trace element and Nd isotopic evidence and implications for crust–mantle relationships. *Earth and Planetary Science Letters* **221**, 293–308.
- Müntener, O. & Piccardo, G. B. (2003). Melt migration in ophiolitic peridotites: the message from Alpine–Apennine peridotites and implications for embryonic ocean basins. In: Dilek, Y. and Robinson, P. T. (eds) *Ophiolites in Earth History*. *Geological Society, London, Special Publications* **218**, 69–89.
- O'Driscoll, B., Donaldson, C. H., Troll, V. R., Jerram, D. A. & Emeeus, C. H. (2007). An origin for harristic and granular olivine in the Rum layered suite, NW Scotland: a crystal size distribution study. *Journal of Petrology* **48**, 253–270.
- Ottoneo, G., Piccardo, G. B. & Ernst, W. G. (1979). Petrogenesis of some Ligurian peridotites—II. Rare earth element chemistry. *Geochimica et Cosmochimica Acta* **43**, 1273–1284.
- Paquet, M., Cannat, M., Brunelli, D., Hamelin, C. & Humler, E. (2016). Effect of melt/mantle interactions on MORB chemistry at the easternmost Southwest Indian Ridge (61°–67°E). *Geochemistry, Geophysics, Geosystems* **17**, 4605–4640.
- Piccardo, G. B. & Guarnieri, L. (2010). Alpine peridotites from the Ligurian Tethys: an updated critical review. *International Geological Review* **52**, 1138–1159.
- Piccardo, G. B. & Vissers, R. L. M. (2007). The pre-oceanic evolution of the Erro–Tobbio peridotite (Voltri Massif, Ligurian Alps, Italy). *Journal of Geodynamics* **43**, 417–449.
- Piccardo, G. B., Rampone, E. & Vannucci, R. (1990). Upper mantle evolution during continental rifting and ocean formation: evidence from peridotites bodies of the Western Alpine–Northern Apennine system. *Mémoires de la Société Géologique de France* **156**, 323–333.
- Piccardo, G. B., Rampone, E. & Vannucci, R. (1992). Ligurian peridotites and ophiolites: from rift to ocean formation in the Jurassic Ligure–Piemontese basin. *Acta Vulcanologica* **2**, 313–325.
- Piccardo, G. B., Müntener, O., Zanetti, A. & Pettke, T. (2004). Ophiolite peridotites of the Alpine–Apennine system: mantle processes and geodynamic relevance. *International Geological Review* **40**, 1119–1159.
- Piccardo, G. B., Zanetti, A. & Müntener, O. (2007). Melt/peridotite interaction in the Southern Lanzo peridotite: field, textural and geochemical evidence. *Lithos* **94**, 181–209.
- Pirard, C., Hermann, J., St O'Neill, H. C. (2013). Petrology and geochemistry of the crust–mantle boundary in a nascent arc, Massif du Sud ophiolite, New Caledonia, SW Pacific. *Journal of Petrology* **54**, 1759–1792.
- Quick, J. E. (1981). Petrology and petrogenesis of the Trinity peridotite, an upper mantle diapir in the eastern Klamath mountains, northern California. *Journal of Geophysical Research* **86**, 11837–11863.
- Quick, J. E. (1982). The origin and significance of large, tabular dunite bodies in the Trinity peridotite, Northern California. *Contributions to Mineralogy and Petrology* **78**, 413–422.
- Rampone, E. & Borghini, G. (2008). Melt migration and intrusion in the Erro–Tobbio peridotites (Ligurian Alps, Italy): insights on magmatic processes in extending lithospheric mantle. *European Journal of Mineralogy* **20**, 573–585.
- Rampone, E. & Piccardo, G. B. (2000). The ophiolite–oceanic lithosphere analogue: new insights from the northern Apennine (Italy). In: Dilek, J., Moores, E., Elthon, D. and Nicolas, A. (eds) *Ophiolites and Oceanic Crust: New Insights from Field Studies and Ocean Drilling Program*. *Geological Society of America, Special Papers* **349**, 21–34.
- Rampone, E., Piccardo, G. B., Vannucci, R., Bottazzi, P. & Ottolini, L. (1993). Subsolidus reactions monitored by trace element partitioning: the spinel- to plagioclase-facies transition in mantle peridotites. *Contributions to Mineralogy and Petrology* **115**, 1–17.
- Rampone, E., Piccardo, G. B., Vannucci, R. & Bottazzi, P. (1997). Chemistry and origin of trapped melts in ophiolitic peridotites. *Geochimica et Cosmochimica Acta* **61**, 4557–4569.

- Rampone, E., Hofmann, A. W. & Raczek, I. (1998). Isotopic contrasts within the Internal Liguride ophiolite (N-Italy): the lack of genetic mantle–crust link. *Earth and Planetary Science Letters* **163**, 175–189.
- Rampone, E., Romairone, A. & Hofmann, A. W. (2004). Contrasting bulk and mineral chemistry in depleted peridotites: evidence for reactive porous flow. *Earth and Planetary Science Letters* **218**, 491–506.
- Rampone, E., Romairone, A., Abouchami, W., Piccardo, G. B. & Hofmann, A. W. (2005). Chronology, petrology and isotope geochemistry of the Erro–Tobbio peridotites (Ligurian Alps, Italy): records of late Paleozoic lithospheric extension. *Journal of Petrology* **46**, 799–827.
- Rampone, E., Piccardo, G. B. & Hofmann, A. W. (2008). Multi-stage melt–rock interaction in the Mt. Maggiore (Corsica, France) ophiolitic peridotites: microstructural and geochemical evidence. *Contributions to Mineralogy and Petrology* **156**, 453–475.
- Rampone, E., Borghini, G., Romairone, A., Abouchami, W., Class, C. & Goldstein, S. L. (2014). Sm–Nd geochronology of the Erro–Tobbio gabbros (Ligurian Alps, Italy): insights into the evolution of the Alpine Tethys. *Lithos* **205**, 236–246.
- Rampone, E., Borghini, G., Godard, M., Ildefonse, B., Crispini, L. & Fumagalli, P. (2016). Melt/rock reaction at oceanic peridotite/gabbro transition as revealed by trace element chemistry of olivine. *Geochimica et Cosmochimica Acta* **190**, 309–331.
- Rampone, E., Borghini, G. & Basch, V. (2018). Melt migration and melt–rock reaction in the Alpine–Apennine peridotites: insights on mantle dynamics in extending lithosphere. *Geoscience Frontiers*, doi: 10.1016/j.gsf.2018.11.001.
- Renna, M. R. & Tribuzio, R. (2011). Olivine-rich troctolites from Ligurian ophiolites (Italy): evidence for impregnation of replacive mantle conduits by MORB-type melts. *Journal of Petrology* **52**, 1763–1790.
- Renna, M. R., Tribuzio, R. & Ottolini, L. (2016). New perspectives on the origin of olivine-rich troctolites and associated harri-sites from the Ligurian ophiolites (Italy). *Journal of the Geological Society, London* **173**, 916–932.
- Renna, M. R., Tribuzio, R., Sanfilippo, A. & Thirlwall, M. (2018). Role of melting process and melt–rock reaction in the formation of Jurassic MORB-type basalts (Alpine ophiolites). *Contributions to Mineralogy and Petrology* **173**, 31.
- Rosenberg, C. L. & Handy, M. R. (2005). Experimental deformation of partially melted granite revisited: implications for the continental crust. *Journal of Metamorphic Geology* **23**, 19–28.
- Ross, K. & Elthon, D. (1997). Cumulus and postcumulus crystallization in the oceanic crust: major and trace elements geochemistry of Leg 153 gabbroic rocks. In: Karson, J. A., Cannat, M. and Miller, D. J. (eds) *Proceedings of the Ocean Drilling Program, Scientific Results*, Vol. **143**. College Station, TX, Ocean Drilling Program, pp. 333–350.
- Saccani, E., Principi, G., Garfagnoli, F. & Menna, F. (2008). Corsica ophiolites: geochemistry and petrogenesis of basaltic and metabasaltic rocks. *Ophioliti* **33**, 187–202.
- Sanfilippo, A. & Tribuzio, R. (2013). Building of the deepest crust at a fossil slow-spreading centre (Pineto gabbroic sequence, Alpine Jurassic ophiolites). *Contributions to Mineralogy and Petrology* **165**, 705–721.
- Sanfilippo, A., Dick, H. J. B. & Ohara, Y. (2013). Melt–rock reaction in the mantle: mantle troctolites from the Parece Vela ancient back-arc spreading centre. *Journal of Petrology* **54**, 861–885.
- Sanfilippo, A., Tribuzio, R. & Tiepolo, M. (2014). Mantle–crust interactions in the oceanic lithosphere: constraints from minor and trace elements in olivine. *Geochimica et Cosmochimica Acta* **141**, 423–439.
- Sanfilippo, A., Morishita, T., Kumagai, H., Nakamura, K., Okino, K., Hara, K., Tamura, A. & Arai, S. (2015a). Hybrid troctolites from mid-ocean ridges: inherited mantle in the lower crust. *Lithos* **232**, 124–130.
- Sanfilippo, A., Tribuzio, R., Tiepolo, M. & Berno, D. (2015b). Reactive flow as dominant evolution process in the lower-most oceanic crust: evidence from olivine of the Pineto ophiolite (Corsica). *Contributions to Mineralogy and Petrology* **170**, 38.
- Sanfilippo, A., Dick, H. J. B., Ohara, Y. & Tiepolo, M. (2016a). New insights on the origin of troctolites from the breakaway area of the Godzilla Megamullion (Parece Vela back-arc basin): the role of melt–mantle interaction on the composition of the lower crust. *Island Arc* **25**, 220–234.
- Sanfilippo, A., Morishita, T. & Senda, R. (2016b). Rhenium–osmium isotope fractionation at the oceanic crust–mantle boundary. *Geology* **44**, 167–170.
- Sanfilippo, A., Tribuzio, R., Ottolini, L. & Hamada, M. (2017). Water, lithium and trace element compositions of olivine from Lanzo South replacive mantle dunites (Western Alps): new constraints into melt migration processes at cold thermal regimes. *Geochimica et Cosmochimica Acta* **214**, 51–72.
- Saper, L. & Liang, Y. (2014). Formation of plagioclase-bearing peridotite and plagioclase-bearing wehrlite and gabbro suite through reactive crystallization: an experimental study. *Contributions to Mineralogy and Petrology* **167**, 985.
- Scambelluri, M., Hoogerduijn Strating, E. H., Piccardo, G. B., Vissers, R. L. M. & Rampone, E. (1991). Alpine olivine and titanian clinohumite bearing assemblages in the Erro–Tobbio peridotites. *Journal of Metamorphic Geology* **9**, 79–91.
- Seyler, M., Cannat, M. & Mével, C. (2003). Evidence for major element heterogeneity in the mantle source of abyssal peridotites from the Southwest Indian Ridge (52° to 68°E). *Geochemistry, Geophysics, Geosystems* **4**, 9101.
- Soustelle, V., Tommasi, A., Bodinier, J. L., Garrido, C. J. & Vauchez, A. (2009). Deformation and reactive melt transport in the mantle lithosphere above a large-scale partial melting domain: the Ronda peridotite massif, Southern Spain. *Journal of Petrology* **50**, 1235–1266.
- Soustelle, V., Tommasi, A., Demouchy, S. & Ionov, D. A. (2010). Deformation and fluid–rock interaction in the supra-subduction mantle: microstructures and water contents in peridotite xenoliths from the Avacha Volcano, Kamchatka. *Journal of Petrology* **51**, 363–394.
- Soustelle, V., Walte, N. P., Geeth, M. A., Manthilake, M. & Frost, D. J. (2014). Melt migration and melt–rock reactions in the deforming Earth’s upper mantle: experiments at high pressure and temperature. *Geology* **42**, 83–86.
- Suhr, G., Hellebrand, E., Johnson, K. & Brunelli, D. (2008). Stacked gabbro units and intervening mantle: a detailed look at a section of IODP Leg 305, Hole U1309D. *Geochemistry, Geophysics, Geosystems* **9**, Q10007.
- Takazawa, E., Frey, F. A., Shimizu, N., Obata, M. & Bodinier, J.-L. (1992). Geochemical evidence for melt migration and reaction in the upper mantle. *Nature* **359**, 55–58.
- Tommasi, A., Mainprice, D., Canova, G. & Chastel, Y. (2000). Viscoplastic self-consistent and equilibrium-based modeling of olivine lattice preferred orientations: implications for the upper mantle seismic anisotropy. *Journal of Geophysical Research: Solid Earth* **105**, 7893–7908.
- Tribuzio, R., Tiepolo, M., Vannucci, R. & Bottazzi, P. (1999). Trace element distribution within olivine-bearing gabbros from the Northern Apennine ophiolites (Italy): evidence for post-cumulus crystallization in MOR-type gabbroic

- rocks. *Contributions to Mineralogy and Petrology* **134**, 123–133.
- Tribuzio, R., Tiepolo, M. & Vannucci, R. (2000). Evolution of gabbroic rocks of the northern Apennine ophiolites (Italy): comparison with the lower oceanic crust from modern slow-spreading ridges. In: Dilek, Y., Moores, E. M., Elthon, D. and Nicolas, A. (eds) *Ophiolites and Oceanic Crust: New Insights from Field Studies and the Ocean Drilling Program. Geological Society of America, Special Papers* **349**, 129–138.
- Tribuzio, R., Thirlwall, M. F. & Vannucci, R. (2004). Origin of the gabbro–peridotite association from the Northern Apennine ophiolites (Italy). *Journal of Petrology* **45**, 1109–1124.
- Tursack, E. & Liang, Y. (2012). A comparative study of melt–rock reactions in the mantle: laboratory dissolution experiments and geological field observations. *Contributions to Mineralogy and Petrology* **163**, 861–876.
- Van den Bleeken, G., Müntener, O. & Ulmer, P. (2011). Melt variability in percolated peridotite: an experimental study applied to reactive migration of tholeiitic basalt in the upper mantle. *Contributions to Mineralogy and Petrology* **161**, 921–945.
- Van der Wal, D. & Bodinier, J.-L. (1996). Origin of the recrystallization front in the Ronda peridotite by km-scale pervasive porous melt flow. *Contributions to Mineralogy and Petrology* **122**, 387–405.
- Visser, R. L. M., Drury, M. R., Hoogerduijn Strating, E. H. & Van der Wal, D. (1991). Shear zones in the upper mantle: a case study in an Alpine lherzolite massif. *Geology* **19**, 990–993.